Journal of Hydrology: Regional Studies 42 (2022) 101120

Contents lists available at ScienceDirect

Journal of Hydrology: Regional Studies

journal homepage: www.elsevier.com/locate/ejrh

Evaluating the uncertainty of climate model structure and bias correction on the hydrological impact of projected climate change in a Mediterranean catchment

Alfonso Senatore [a,*], Domenico Fuoco [a], Mario Maiolo [a], Giuseppe Mendicino [a], Gerhard Smiatek [b], Harald Kunstmann [b,c]

[a] Department of Environmental Engineering, University of Calabria, Rende (CS), Italy
[b] Institute of Meteorology and Climate Research Atmospheric Environmental Research (IMK-IFU), KIT Campus Alpin, Garmisch-Partenkirchen, Germany
[c] Institute of Geography, University of Augsburg, Augsburg, Germany

ARTICLE INFO

Keywords:
Climate change hydrological impact
GCM-RCM combinations
Change factor
Bias correction
ANOVA
Mediterranean catchments

ABSTRACT

Study region: Crati River Basin, Southern Italy, Central Mediterranean.
Study focus: We evaluate the combined effect of multiple global and regional climate model (GCM-RCM) combinations and bias correction (BC) methods on the hydrological impact of projected climate change. Under the representative concentration pathway RCP4.5, 15 EURO-CORDEX members, combining 6 GCMs and five high-resolution (0.11°) RCMs, provide the meteorological input for a spatially distributed hydrological model. RCM-derived input data are uncorrected and corrected through three empirical methods, leading to 60 different simulations for three ~30-year future periods in 2020–2096, compared to the baseline 1975–2005. The combined uncertainty of the climate models and correction methods is evaluated for the main hydrological variables using an analysis of variance (ANOVA) method.
New hydrological insights for the region: Results highlight a considerable agreement in projecting a decreasing trend of available water resources (on average, −70 % for snow, −8 % for root zone soil moisture and −17 % for river runoff in the period 2070–2096), due to the remarkable mean temperature increase and less accentuated precipitation reduction. The uncertainty evaluation shows that (1) the primary source of uncertainty is the driving GCM, and (2) BC methods smooth the projected hydrological impact in a not negligible way, especially concerning discharge (for each future period, the reduction projected without bias correction is about 3 % higher than with BC), therefore contributing to the total uncertainty.

1. Introduction

The studies on the hydrological impact of climate change must cope with the uncertainty arising from the complex modelling chain leading to hydrological projections. A cascade of uncertainty proceeds from the envisaged future socio-economic scenarios and related greenhouse gas emissions down to the modelling of adaptation responses (Wilby and Dessai, 2010). In the middle, further high uncertainty arises from the structure and parameterisation of the models used at different resolutions to project climate change, from the

* Corresponding author.
E-mail address: alfonso.senatore@unical.it (A. Senatore).

https://doi.org/10.1016/j.ejrh.2022.101120
Received 7 November 2021; Received in revised form 23 May 2022; Accepted 25 May 2022
Available online 3 June 2022

global climate models (GCMs), to statistical or dynamical (through regional climate models, RCMs) downscaling methods, down to the hydrological models (Dobler et al., 2012; Gobiet et al., 2014).

In the last decade, several studies investigated the uncertainty linked to model projections, analysing the interactions of the single sources of uncertainty and evaluating the relative weight of each source (see Ashraf Vaghefi et al., 2019 for a review). While most analyses consistently recognised GCMs as the primary sources of uncertainty (Chen et al., 2013), there is no general agreement about the relative importance of the other components of the modelling chain.

To assess the hydrological impact, especially in small- to medium-size catchments (maximum area in the order of $\sim 10^3$ km^2), downscaling the coarse-resolution information provided by GCMs is an inevitable step. Dynamical downscaling methods (i.e., RCMs) use consistently the same fundamental physical principles driving the GCMs (Gutmann et al., 2012). Furthermore, comprehensive investigation of the interrelated uncertainties descending from GCMs to RCMs is supported by the Coordinated Regional Downscaling Experiment (CORDEX, Giorgi et al., 2009; Giorgi and Gutowski, 2015), an intercomparison project focused on regional modelling, which addresses specific world regions with targeted initiatives like, e.g., EURO-CORDEX (Jacob et al., 2014) dealing with the European continent.

Despite their capability of providing physically-based high-resolution information about all the climate variables simulated by GCMs, RCMs' performances are subject to some limitations. Such limitations must be considered when these models are intended for further use in impact studies (e.g., Xie et al., 2015; Maraun et al., 2010; Maraun, 2013; Senatore et al., 2011; Mascaro et al., 2018). Therefore, the most relevant RCM variables used as inputs need corrections through a proper strategy for hydrological studies. Ho et al. (2012) identified two main calibration pathways in the change factor, and the bias correction approaches. With the former, observations are modified with the modelled climate change signal (CCS) to derive future scenarios, while with the latter future projections are corrected using the model bias calculated against observations. Despite this distinction, in practice, many authors refer to change factor methods as particular bias correction methods (e.g., Teutschbein and Seibert, 2013), therefore hereafter, we will refer to "bias correction", including also change factor methods. Furthermore, according to Potter et al. (2020), bias correction methods can be grouped in scaling or change factor methods and either non-parametric (empirical) or parametric (distributional) quantile-quantile-mapping (QQM).

The assumptions on which the different bias correction approaches rely are debatable. Many studies addressed basic questions concerning their effects and potential benefits (e.g., Maraun et al., 2017). The main concerns regard the physical justification of applying such methods (Ehret et al., 2012), whether bias correction can be applied directly to GCMs (Ngai et al., 2017), and the possibility of application for non-stationary conditions (Teutschbein and Seibert, 2013). Likewise, it is debated to what extent bias correction provides a more consistent representation of river runoff for the past and how much it acts as a source of uncertainty, affecting the estimation of future change in hydrological indicators (Muerth et al., 2013), including extreme values (Willkofer et al., 2018). Furthermore, some techniques could not correctly preserve changes in quantiles and extremes (Cannon et al., 2015) or could affect modelled runoff (Teng et al., 2015). Finally, further uncertainty can arise from the accuracy of the observational datasets on which bias correction relies (Kim et al., 2015) and the periods used for calibration (Chen et al., 2015; Gampe et al., 2019).

Bias correction methods represent another source of uncertainty in the framework of the overall modelling chain under non-stationary conditions. Therefore, the impact of the choice of different bias correction methods on hydrological output is being increasingly investigated (e.g., Chen et al., 2013; Muerth et al., 2013; Huang et al., 2014; Fang et al., 2015; Teng et al., 2015; Seaby et al., 2015; Johnson and Sharma, 2015; Li et al., 2019), also with the aid of techniques for the analysis of the variance (Al Aamery et al., 2016; Aryal et al., 2019; Ashraf Vaghefi et al., 2019; Meresa et al., 2021; Lee et al., 2022). Such an impact on the relative climate change signal is generally weak, but some studies (e.g., Johnson and Sharma, 2015; Al Aamery et al., 2016) found that bias correction mitigates the change projected by raw model simulations. Others, e.g. Aryal et al. (2019) or Meresa et al. (2021), highlighted the contribution to the total uncertainty of combined driving climate models and bias correction methods.

Uncertainty evaluation of future projections is particularly relevant for highly vulnerable regions to climate change, such as the Mediterranean Basin (Giorgi and Lionello, 2008; IPCC, 2014; Garrote et al., 2015; Cramer et al., 2018; Tuel and Eltahir, 2020), which is mainly affected by drought risk (Cook et al., 2014; Hoegh-Guldberg et al., 2018; Tramblay et al., 2020). In this area, anthropogenic greenhouse gas emissions are likely contributing to an increase in the occurrence of dry spells, enhancing this trend with ever-higher levels of global warming (Gudmundsson et al., 2017). The consequences on the hydrological cycle of the observed and projected change in the precipitation and temperature regimes in the Mediterranean affect the whole ecosystem and, consequently, essential socio-economic activities, like drinking water distribution (UN, 2021; Maiolo et al., 2017), food production (FAO, 2016; Ronco et al., 2017) or preparedness to hydrometeorological extremes (Madsen et al., 2014). Therefore, in the last years, the climate change impact studies dealing with the projected hydrological variability in Mediterranean catchments has increased tremendously, addressing either the whole region (e.g., Hertig and Tramblay, 2016, Hartmann et al., 2017) or smaller areas (e.g., Spain: Estrela et al., 2012; Majone et al., 2012; Olmos Giménez et al., 2016; France: Lafaysse et al., 2014; Prats et al., 2018; Dayon et al., 2018; northern Africa: Beyene et al., 2010; Sellami et al., 2016; Taïbi et al., 2019; Hadour et al., 2020; Greece: Tigkas et al., 2012; Koutroulis et al., 2013; Nerantzaki et al., 2020; Middle East: Smiatek et al., 2014; Bucak et al., 2017; Gorguner et al., 2019; Italy: Senatore et el., 2011; Ravazzani et al., 2015; Pumo et al., 2016; Majone et al., 2016; Perra et al., 2018; D'Oria et al., 2019; Peres et al., 2019; Citrini et al., 2020).

This study aims to contribute to the ongoing debate about uncertainty in projecting climate change hydrological impact, addressing the portion of the overall modelling chain composed by the global and regional models and further bias correction, which is applied to both precipitation and temperature, the main input variables of several hydrological models. Our fundamental exercise is demonstrated in the Crati River Basin, a typical Mediterranean catchment located in Southern Italy. The hydrological impact analysis under climate change in this basin was already performed by Senatore et al. (2011), considering three RCMs and the period 2070–2099 with SRES emission scenarios (Nakícenovíc et al., 2000). In this study, the climate change scenario ensemble includes 15 members deriving

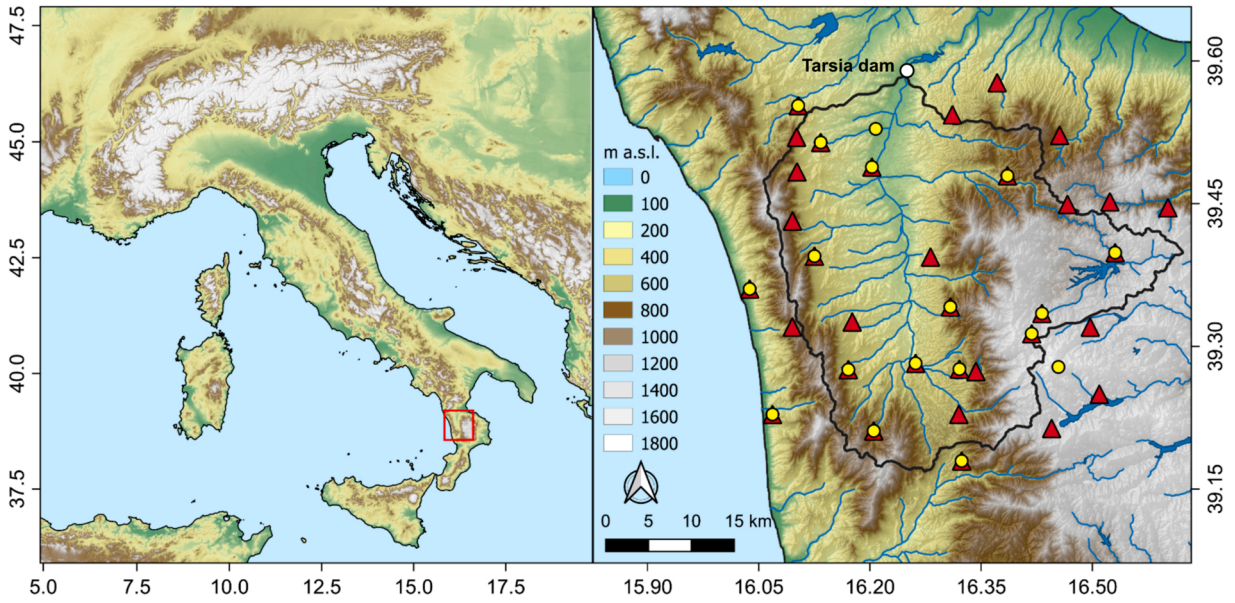

Fig. 1. Study area in the context of the Italian peninsula. In the figure on the right, the black contours highlight the borders of the Crati River Basin, the yellow circles indicate thermometers, the red triangles the rain gauges, and the white circle the location of the Tarsia Dam. (For interpretation of the references to colour in this figure, the reader is referred to the web version of this article.)

from the combination of 6 GCMs and 5 high-resolution (0.11°) RCMs in the framework of the EURO-CORDEX project. The variables of interest are uncorrected and corrected through three bias correction methods representative of change factor, scaling and quantile-quantile-mapping methods, and then used as the input for the fully distributed Intermediate Space-Time Resolution Hydrological Model (In-STRHyM; Senatore et al., 2011). Our previous study results are updated and enlarged because projected change under a representative concentration pathway (RCP4.5, namely; Van Vuuren et al., 2011) spans the whole period from 2020 to 2096, subdivided into 2020–2049, 2040–2069 and 2070–2096. Furthermore, they are generalisable in terms of uncertainty evaluation. The extra level of uncertainty introduced by different correction methods is quantified and related, for each ~30-year scenario, to that originated by the different GCM-RCM combinations on several relevant variables, such as groundwater and root zone water content, evapotranspiration, and river runoff.

2. Data and methods

2.1. Study area

The study focuses on the Crati River Basin (Fig. 1), the largest in the Calabria region (southern Italy). The analysed area is delimited by the Sila plateau (East and South) and the Tyrrhenian coastal chain (West), with the closing section (North) at the Tarsia dam. The average altitude of the study area, determined on a 20 m resolution digital terrain model (DTM), is approximately 682 m a.s.l., with a maximum of 1781 m a.s.l. in the Sila plateau and a minimum of 52 m a.s.l. at the closing section. The contributing area has an extension of 1280 km^2 and a perimeter of about 190 km, while the main river channel is 52 km long.

Vegetation cover was considered constant during the whole study period (even the future), emphasising changes due only to CCS. Reference land cover was taken from the Corine Land Cover 2000 project. The primary land cover types in the basin are forests (43 %, with 26 % broad-leaved forest) and agricultural areas (47 %, with 14 % non-irrigated arable land and 12 % olive groves).

Precipitation and temperature measurements are performed through a monitoring network of 33 rain gauges and 18 thermometers. As for climate conditions, according to the Thornthwaite (1948) classification, the Crati River basin is characterised by a Mediterranean climate from sub-humid to hyper-humid. For the period 1975–2005, which is considered as the baseline for the evaluation of climate change scenarios, the cumulative precipitation is approximately 1100 mm $year^{-1}$, with monthly mean values ranging from a minimum of 27 mm $month^{-1}$ in summer (JJA) to a maximum of 142 mm $month^{-1}$ in winter (DJF). For the same period, the average monthly temperature ranges from 5 °C in winter to 21 °C in summer, with an average annual value of approximately 14 °C.

2.2. EURO-CORDEX RCMs

The meteorological variables used as input in the hydrological analysis for the projection of water resources variability, i.e. precipitation, temperature and net radiation, are determined from the output of 15 RCMs provided through the EURO-CORDEX initiative (Jacob et al., 2014). In the framework of EURO-CORDEX, several GCMs derived from the CMIP5 project (Coupled Model

Table 1
List and acronyms of GCM-RCM combinations used in this study. [1G] Voldoire et al. (2013), Centre National de Recherches Météorologiques; [2G] Hazeleger et al. (2010), Irish Centre for High-End Computing, EC-Earth Consortium, Europe; [3G] Collins et al. (2011), Met Office Hadley Centre; [4G] Dufresne et al. (2013), Institut Pierre Simon Laplace; [5G]: Giorgetta et al. (2013), Max-Planck-Institute für Meteorologie; [6G]: Bentsen et al. (2013), Iversen et al. (2013), Norwegian Earth System Model; [1R] Strandberg et al. (2014), Swedish Meteorological and Hydrological Institute, Rossby Centre; [2R] Baldauf et al. (2011), Rockel et al. (2008), Climate Limited-area Modelling Community (CLM-Community); [3R] Christensen et al. (2007), Danish Meteorological Institute; [4R] van Meijgaard et al. (2008), Royal Netherlands Meteorological Institute, De Bilt, The Netherlands; [5R] Teichmann et al. (2013), Helmholtz-Zentrum Geesthacht, Climate Service Center, Max Planck Institute for Meteorology.

GCM	RCM	Model acronym
CNRM-CERFACS-CNRM-CM5[1G]	SMHI-RCA4[1R]	CM5RCA4
ICHEC-EC-EARTH[2G]	CLMcom-CCLM4–8–17[2R]	ECECCLM
ICHEC-EC-EARTH	DMI-HIRHAM5[3R]	ECEHIRH
ICHEC-EC-EARTH	KNMI-RACMO22E[4R]	ECERACM
ICHEC-EC-EARTH	KNMI-RACMO22E	ECERACMr12
ICHEC-EC-EARTH	SMHI-RCA4	ECERCA4
MOHC-HadGEM2-ES[3G]	CLMcom-CCLM4–8–17	HadCCLM
MOHC-HadGEM2-ES	KNMI-RACMO22E	HadRACM
MOHC-HadGEM2-ES	SMHI-RCA4	HadRCA4
IPSL-IPSL-CM5A-MR[4G]	SMHI-RCA4	IPSRCA4
MPI-M-MPI-ESM-LR[5G]	CLMcom-CCLM4–8–17	MPICCLM
MPI-M-MPI-ESM-LR	SMHI-RCA4	MPIRCA4
MPI-M-MPI-ESM-LR	MPI-CSC-REMO2009[5R]	MPIREMO
MPI-M-MPI-ESM-LR	MPI-CSC-REMO2009	MPIREMOr2
NCC-NorESM1-M[6G]	DMI-HIRHAM5	NorHIRH

Intercomparison Phase 5; Taylor et al., 2012) were dynamically downscaled. RCMs resolution is currently the highest for downscaling within CORDEX, i.e. 0.11°. Since this study focuses on the uncertainty provided by different GCM-RCM chains and bias correction methods, only the output of the intermediate scenario RCP4.5 is selected. This scenario reflects the more plausible outcomes given the current (and pledged) policies (Hausfather and Peters, 2020). For each of the 15 models, simulations outputs in the control period 1975–2005 and projection period 2020–2096 are used. Table 1 shows the models used, renamed through an acronym consisting of three letters referring to the GCM name and four to the RCM name. Furthermore, when more than one ensemble member belongs to the same GCM-RCM combination, the suffix *r* (an abbreviation for 'realisation') followed by a number given by the institute running the GCMs is used.

2.3. The hydrological model In-STRHyM

The hydrological analysis is conducted using the In-STRHyM model (Intermediate Space-Time Resolution Hydrological Model; Senatore et al., 2011). In-STRHyM is a fully distributed hydrological model developed to analyse hydrological processes on small-medium sized Mediterranean basins, designed to work at "intermediate" spatial and temporal resolutions (1 km and 24 h, respectively) particularly suitable for long-range analyses. It reproduces all the main surface and subsurface hydrological processes, i.e.: snow accumulation and melting (following the scheme proposed by the SWAT model, Neitsch et al., 2002, which distinguishes rainfall and snow depending on a threshold temperature); interception (Kriestensen and Jensen, 1975); infiltration and soil water redistribution along the soil column (using a gravitational method which allows water movement along the root zone, an unsaturated layer below the root zone and the water table, exfiltration and runoff generation); actual evapotranspiration (using the approach proposed by Allen et al., 1998, with a crop coefficient and a water stress coefficient accounting for land cover type and the actual root zone water content, respectively; furthermore, contributions from vegetated and bare soil are separated, and the reference evapotranspiration is calculated following Priestley and Taylor, 1972); base flow routing (following a two-dimensional approach); and surface and sub-surface flow routing (kinematic cascade approach). Therefore, the model output provides daily maps of snow accumulation, evapotranspiration, root zone soil moisture and storage in an idealised near-surface groundwater layer, and the simulated runoff at the closing section as a time series.

In-STRHyM was calibrated for the Crati River Basin over available daily discharge values at the closing section during 1961–1966, achieving a Nash-Sutcliffe coefficient value of 0.83 (Senatore et al., 2011). Subsequent validation over the periods 1969–1971 and 2004–2006 (no other discharge data are available) led to Nash-Sutcliffe coefficient values of 0.64 and 0.57, respectively. This study's original model was updated by migrating the code from Visual Basic using Map Window GIS Activex Control extension to Python with GDAL/OGR Geospatial Data Abstraction software Library. The new version of the model allows for more efficient parallelised calculations.

The model's meteorological input data is provided through spatial interpolating point values acquired by either the observational network or the RCMs. In the latter, cells centres falling within and in the neighbouring of the study area are considered. The daily maps of precipitation are achieved through spline interpolations; temperature maps are obtained by integrating the spline interpolation with daily elevation-dependent regressions, thus accounting for the influence of the orography. Concerning net radiation, RCM values are determined from the balance of the incident and reflected short- and long-wave radiations and then interpolated in the same way as precipitation. At the same time, the output from a modified version of a model by Moore et al. (1993) replaces missing observations.

Due to the lack of measurements, this variable is not bias-corrected.

Further details about interpolation methods and other input parameters are provided by Senatore et al. (2011). The meteorological input grids are returned at a resolution of 1 km, both for the reference (1975–2005) and projection periods (2020–2096).

2.4. Bias correction methods

Considering both uncorrected (NB, meaning 'no bias correction') and corrected RCMs' precipitation and temperature fields, the hydrological projections are performed. Three approaches are used for correction, namely: (1) the constant scaling method (CS; Mpelasoka and Chiew, 2009; Chen et al., 2011; Chen et al., 2013), a change factor approach; (2) the method proposed by Kunstmann et al. (2004) (abbreviated with KU hereafter), which can be classified as a scaling bias correction method; and (3) a non-parametric quantile mapping method (QM; Wilks, 1995; Themeßl et al., 2011, 2012; Chen et al., 2013). These methods are briefly detailed in Appendix A.

2.5. Uncertainty evaluation

The variability produced by the use of 15 GCM-RCM combinations and 4 change factor/bias correction approaches (including no correction) in the Crati River Basin is evaluated through the comparison of the 60 projected changes (time-averaged variables) in evapotranspiration, root zone water content, groundwater, and river runoff in the three future periods 2020–2049, 2040–2069 and 2070–2096, considering the whole year, the irrigation period April-September and the four seasons (i.e., DJF, MAM, JJA and SON). Comparisons for all variables are performed by computing the percentage differences, defined as the ratio between (1) the differences of the variable in future scenarios and the control period, and (2) the variable in the control period. Furthermore, the contribution of the two different sources of uncertainty to the total predicted uncertainty of the projected variables is evaluated through an analysis of variance method (ANOVA) following the methodology proposed by Ashraf Vaghefi et al. (2019).

First, for each variable, the total sum of squared errors SSE is determined:

$$SSE = \sum_{i=1}^{N_{GR}} \sum_{j=1}^{N_{BC}} \left(X_{ij} - \overline{X}_{oo}\right)^2 \tag{1}$$

where $N_{GR} = 15$ is the number of combined GCM-RCM projections used, $N_{BC} = 4$ the number of bias correction methods, X_{ij} the value of the hydrological variable X corresponding to the GCM-RCM i and the correction method j, and finally $\overline{X}_{oo}$ is the overall mean.

SSE can be considered as the sum of single contributions to errors given by GCM-RCM combinations (SS_{GR}), bias correction methods (SS_{BC}) and their interaction ($SS_{GR\times BC}$):

$$SSE = SS_{GR} + SS_{BC} + SS_{GR\times BC} \tag{2}$$

$$SS_{GR} = N_{BC} \sum_{i=1}^{N_{GR}} \left(\overline{X}_{io} - \overline{X}_{oo}\right)^2 \tag{3}$$

$$SS_{BC} = N_{GR} \sum_{j=1}^{N_{BC}} \left(\overline{X}_{oj} - \overline{X}_{oo}\right)^2 \tag{4}$$

$$SS_{GR\times BC} = \sum_{i=1}^{N_{GR}} \sum_{j=1}^{N_{BC}} \left(X_{ij} - \overline{X}_{io} - \overline{X}_{oj} + \overline{X}_{oo}\right)^2 \tag{5}$$

The subscript o is used in the previous equations when the average over a specific i or j index is indicated.

To avoid biases in the results of uncertainty decomposition due to the different sizes of GR and BC populations (15 and 4, respectively), the approach of Bosshard et al. (2013) is followed. According to this methodology, all the 1365 possible combinations of 4 (i.e., the BC population size) out of 15 GCM-RCM projections are sampled. Then, for each 4-member sample set m out of 1365, the terms $SS_{GR,m}$, $SS_{BC,m}$ and $SS_{GR\times BC,m}$ are calculated using Eqs. (3–5) (in this case, $N_{GR} = 4$) and their ratios against the corresponding SSE_m are averaged over the whole sample set to achieve the 'unbiased variance fraction' NSS related to each of the single contributions to errors:

$$NSS_U = \frac{1}{1365} \sum_{m=1}^{1365} \frac{SS_{U,m}}{SSE_m} \quad \forall \quad U \in \quad [GR, ED, GR \times BC] \tag{6}$$

The variance decomposition is applied to all the projected hydrological variables for the three future periods. Furthermore, thanks to the flexibility of the method, two subsets of EURO-CORDEX projections, characterised by the coupling of the same GCM with different RCMs and vice versa, are also analysed to provide insights concerning the separated contribution to uncertainty of GCMs and RCMs. Specifically, two experiments were performed, one involving four projections with the same GCM (namely, ECECCLM, ECE-HIRH, ECERACM and ECERCA4, sharing the ICHEC-EC-EARTH GCM; Table 1) and one involving the same RCM (namely, CM5RCA4, ECERCA4, HadRCA4 and MPIRCA4, sharing the SMHI-RCA4 RCM; Table 1).

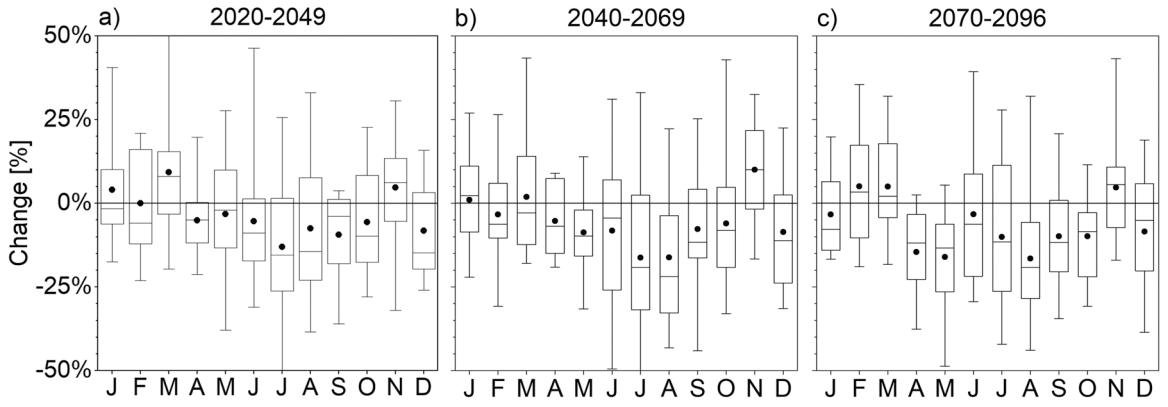

Fig. 2. Projected changes in mean (spatially averaged) monthly precipitation: a) 2020–2049; b) 2040–2069; c) 2070–2096. The box and whiskers plots account for combined GCM-RCM models' variability for each month and projection period. The black dots indicate models' means.

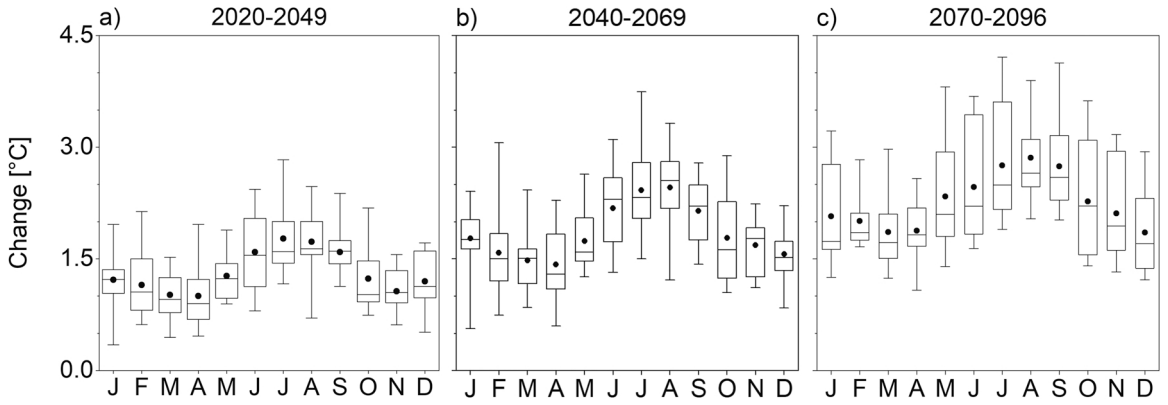

Fig. 3. Same as Fig. 2, but with mean monthly temperature.

3. Results

3.1. Precipitation and temperature

Precipitation and temperature mean values provided by each RCM for the entire projection period 2020–2096 are divided into three different ~30-year intervals (2020–2049, 2040–2069, 2070–2096) compared with the reference period 1975–2005. Changes are evaluated with respect to the reference period for each RCM without considering any bias correction techniques. Precipitation is analysed in percentage variation and temperature as deviation from the reference period. The analysis is performed from a single month to a yearly scale.

The box and whiskers plots in Figs. 2 and 3 show the monthly variability in the projected RCM outputs. For each model, the spatially averaged values are considered. Concerning precipitation (Fig. 2), for most of the months in all the three periods, the models project reductions on average (black dots), except for March, November and, partially, January and February, which typically are rainy months in the Mediterranean climate. However, in no months did all the models agree on reductions. Starting from a reference annual value of 1124 mm, yearly variations range from − 9.4 % to + 4.8 % in 2020–2049, from − 8.5 % to + 2.6 % in 2040–2069 and from − 15.9 % to + 2.1 % in 2070–2096. Projected yearly changes are positive in 4, 1 and 1 cases out of 15, in 2020–2049, 2040–2069 and 2070–2096, respectively. Table S1 goes into details about yearly, irrigation period and seasonal variations, showing that, in general, for each season and period, considerable decreases are projected.

The temperature change signal is much clearer than the precipitation change signal. Fig. 3 shows that a temperature increase is expected in all cases (all models, all periods, all months), with higher growth in summer and moving into the future. Starting form a reference annual value of 12.1 °C, yearly variations range from + 0.9 °C to + 1.9 °C in 2020–2049, from + 1.2 °C to + 2.5 °C in 2040–2069 and from + 1.7 °C to + 3.1 °C in 2070–2096. In summer (JJA, reference value of 20.2 °C), the temperature increase is projected up to + 3.9 °C in 2070–2096.

The reliability of the climate projections can be linked to models' skills in reproducing the current climate. Based on this assumption, weighting procedures can be used to prioritise the most accurate models (e.g., Senatore et al., 2019). None of the models used in this study can perfectly reproduce the reference period's average conditions. Fig. 4 shows the uncertainty of precipitation

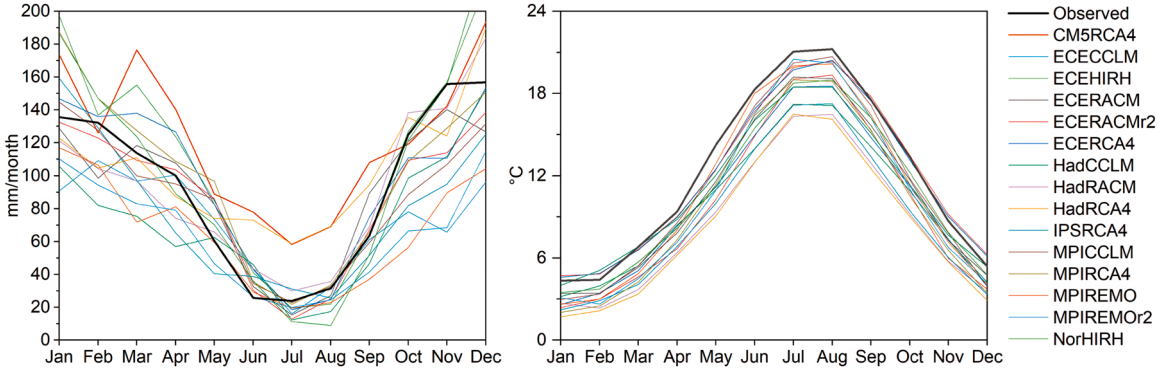

Fig. 4. Simulated and observed mean monthly precipitation (a) and temperature (b) in the control period 1975–2005.

Table 2
Performance indices of mean monthly precipitations and temperatures simulated by the 15 GCM-RCM combinations. MAE is the mean absolute error, and the bias is calculated by subtracting observations to model outputs; R^2 is the coefficient of determination.

Models	P			T		
	MAE (mm d^{-1})	Bias (mm d^{-1})	R^2	MAE (°C)	Bias (°C)	R^2
CM5RCA4	1.09	+ 0.95	0.88	2.40	-2.40	0.99
ECECCLM	0.89	−0.72	0.79	2.07	-2.07	1.00
ECEHIRH	0.67	+ 0.60	0.95	2.33	-2.33	1.00
ECERACM	0.47	−0.10	0.94	3.59	-3.59	1.00
ECERACMr12	0.40	− 0.20	0.95	3.87	-3.87	1.00
ECERCA4	0.53	+ 0.12	0.92	3.18	-3.18	1.00
HadCCLM	0.84	− 0.71	0.91	1.10	-1.10	1.00
HadRACM	0.50	- 0.06	0.94	2.26	-2.26	1.00
HadRCA4	0.81	+ 0.32	0.92	1.34	-1.34	1.00
IPSRCA4	0.74	− 0.50	0.88	1.76	-1.76	0.99
MPICCLM	0.50	−0.26	0.92	1.51	-1.51	1.00
MPIRCA4	0.52	+ 0.24	0.92	1.62	-1.62	1.00
MPIREMO	0.92	− 0.90	0.90	0.71	-0.29	0.99
MPIREMOr2	0.96	−0.96	0.90	0.67	-0.37	1.00
NorHIRH	0.63	+ 0.30	0.94	1.41	-1.30	1.00

simulations, some of which cannot fully represent the typical seasonal variability of the Mediterranean climate, and also shows the substantial temperature underestimation of all models. Table 2 shows some performance indices calculated monthly. The models with the best performances concerning precipitation (i.e., ECERACMr12 with the lowest mean absolute error -MAE- and the highest coefficient of determination R^2, and HadRACM with the lowest absolute bias) are not within the best models considering the temperature. These results, consistent with the analysis performed by Peres et al. (2020) with a broader ensemble of EURO-CORDEX models for a larger area of Southern Italy, highlight the inaccuracies and uncertainties of the GCM-RCM combinations in reproducing the current climate and solicits the use of bias correction methods. These techniques are applied to the precipitation and temperature fields before their use as input in the hydrological model, whose results are shown in the following sections.

3.2. Snow

Starting from this section on snow projections and for the following ones dedicated to specific hydrological variables, results are presented considering the whole set of available models to account for the global uncertainty of the climate change projections. Concurrently, we also focus on a single model to provide an example of the space-time variations due to the bias correction methods. Our choice on which projection to use as an example fell on the HadRACM model, which is the one with the lowest precipitation bias compared to observations (Table 2). A comparison of the mean monthly evolution of the main components of the water balance as simulated by the HAdRACM model with and without bias correction and the corresponding results achieved with the calibrated hydrologic model forced by observations in the control period 1975–2005 is provided as supplementary material (Fig. S1). While, in the following, percentage changes are shown, Fig. S1 also provides absolute values as a reference (furthermore, the annual means of the variables achieved with observation forcing are provided in the main text).

Snow accumulation (in snow water equivalent units) projections mainly pertain to the winter months. Fig. 5 shows the average daily percentage decrease in the three periods 2020–2049, 2040–2069, 2070–2096 compared with the reference period 1975–2005 using the HadRACM model. Some spikes can be noted in the curves, especially at the very beginning and end of the cold season, because of numeric issues (i.e., the absolute values of accumulated snow are minimal). Still, they do not overshadow the primary trend.

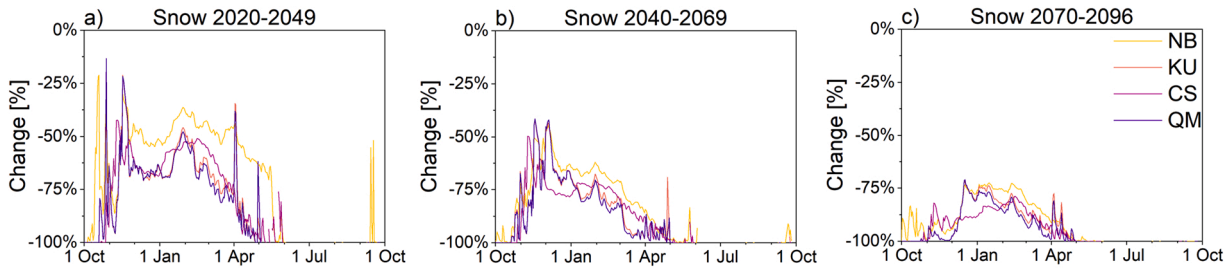

Fig. 5. Average daily percentage changes in snow accumulation using the HadRACM model and four different bias correction methods for the thirty-year periods (a) 2020–2049, (b) 2040–2069 and (c) 2070–2096. NB: no corrections; KU: method proposed by Kunstmann et al. (2004); CS: constant scaling; QM: non-parametric quantile mapping.

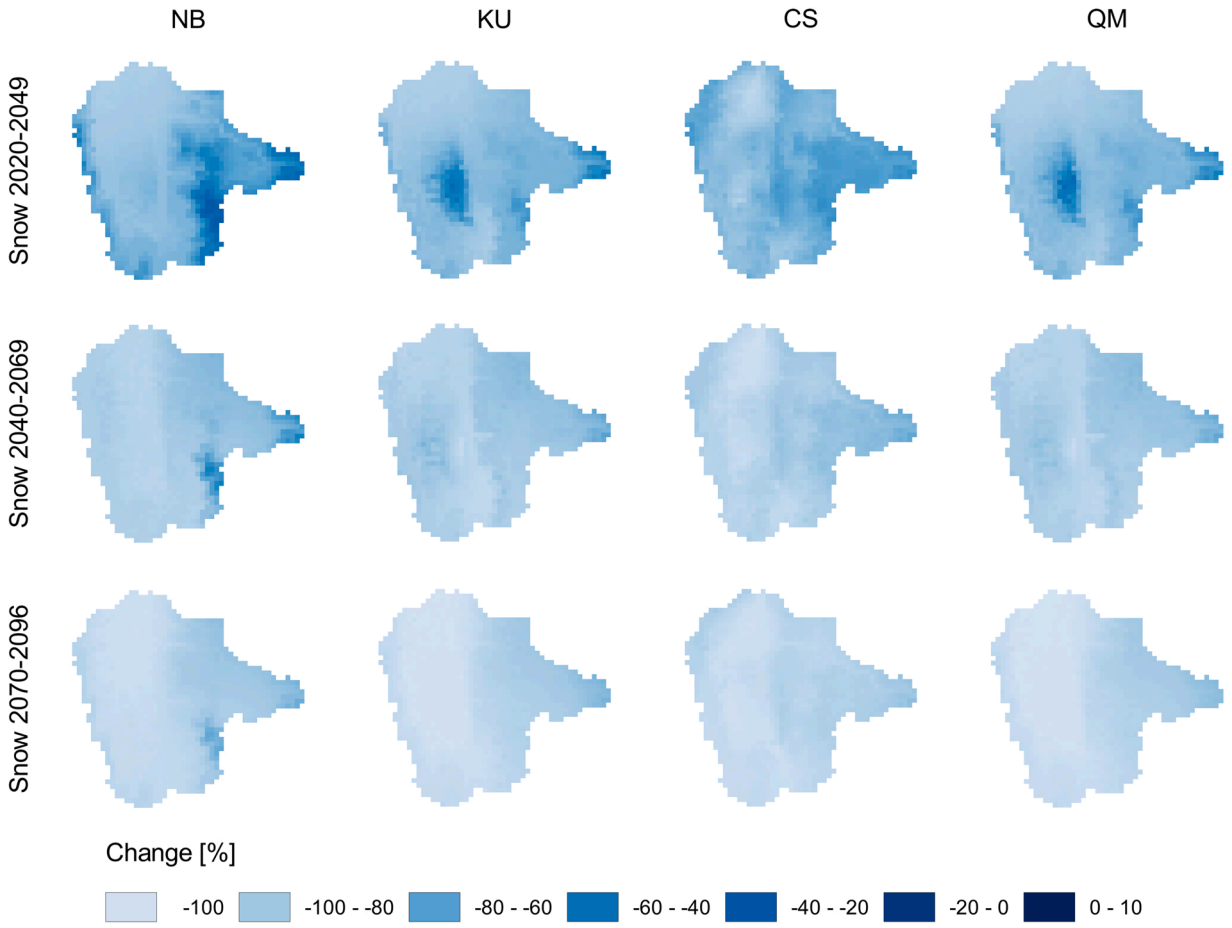

Fig. 6. Spatial distribution of snow accumulation changes compared to the control period 1975–2005 in the Crati River Basin with HadRACM. 1st, 2nd and 3rd rows relate to 2020–2049, 2040–2069 and 2070–2096, respectively. 1st, 2nd, 3rd and 4th columns refer to NB, KU, CS and QM methods, respectively.

The reduction across the three periods is evident mainly due to temperature increases. The simulations using the uncorrected precipitation and temperature fields (labelled with NB) provide a less pronounced (but still relevant) reduction. In contrast, the KU and QM simulations, which use the same correction for temperature, show somewhat similar behaviour.

Fig. 6 focuses on the average spatial distribution of the decrease for the same model HadRACM with different corrections and periods. The main differences concern the period 2020–2049. NB simulation projects a lower decline in the high-altitude areas (especially the Sila plateau in the east). In contrast, KU and QM simulations project a lower decrease in the valley, where snow accumulation is already low in the reference period. The outcomes are more consistent for the other future periods, with the NB simulations projecting a slightly lower decrease on the mountains, agreeing with Fig. 5.

Table 3
Percentage changes in yearly snow accumulation for different corrections and future periods. The first number is the average change of the 15 GCM-RCM models for each combination, while the number in the brackets refers only to the HadRACM model.

	2020–2049	2040–2069	2070–2096
NB	−47.39 (−47.10)	−61.29 (−71.10)	−68.69 (−79.64)
KU	−50.45 (−62.65)	−60.67 (−76.46)	−68.42 (−81.88)
CS	−51.84 (−59.26)	−63.78 (−75.84)	−70.42 (−85.43)
QM	−51.52 (−64.28)	−63.76 (−77.71)	−70.74 (−83.55)

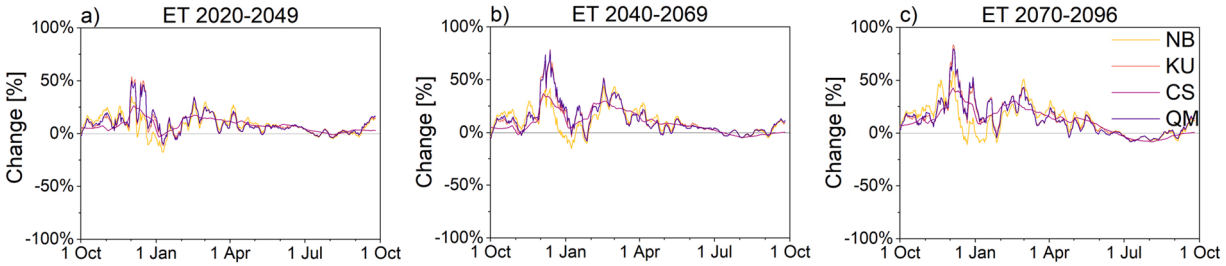

Fig. 7. Same as Fig. 5, but for ET.

Table 4
Same as Table 3, but for yearly ET.

	2020–2049	2040–2069	2070–2096
NB	+ 1.33 (+5.78)	+ 1.78 (+6.72)	+ 1.29 (+6.16)
KU	+ 1.20 (+5.70)	+ 1.49 (+6.39)	+ 0.94 (+5.67)
CS	+ 0.90 (+6.08)	+ 1.20 (+5.36)	+ 0.50 (+5.15)
QM	+ 1.19 (+5.52)	+ 1.60 (+6.15)	+ 1.31 (+5.22)

A summary of yearly snow accumulation percentage changes concerning both HadRACM and the average of all the 15 models is shown in Table 3. Detailed information for each model is provided in Table S3. Models' trends are consistent, with projected decreases (starting from a spatially averaged reference annual value of snow water equivalent in the basin of 65 mm) of approximately 50 %, 60 % and 70 % in the periods 2020–2049, 2040–2069 and 2070–2096, respectively. HadRACM projects a more remarkable decrease, especially in 2070–2096 with the CS simulations. In general, models' agreement is confirmed by the not too high variability of the outputs (total standard deviation values lower than 15 % for every period). Of course, no model in any scenario projects snow accumulation increase.

3.3. Evapotranspiration

Fig. 7 shows the average daily percentage changes of actual evapotranspiration (ET) with HadRACM. As summarised by Table 4, an ET increase is projected for every correction method and every period. In particular, ET increases in 2020–2049, where both precipitation and temperature increase is projected, and in 2040–2069 and 2070–2096, where only temperature increase is projected. Despite the increasing temperatures, a lower ET increase in 2070–2096 than 2040–2069 indicates higher water stress, i.e., less water available for evapotranspiration due to reduced precipitation. The yearly ET increase is generally uniformly distributed in space, even though it is slightly more pronounced in 2070–2096 on the eastern side (Fig. S2).

The same increasing trend found at the yearly scale occurs in the irrigation (April-September) period and even in summer (Tables S4-S7), except in 2070–2096, where ET decrease is projected with all bias correction methods. This behaviour is due to increased water shortage, highlighting higher water stress for the vegetation.

The yearly average trend of all models is positive, like HadRACM, but less pronounced (Table 4). The NB simulations almost always provide the highest average increase. The annual reference value for the control period is approximately 740 mm. All projections for all models and correction methods considering the whole year are shown in Fig. 8. Models outputs are consistent at the yearly scale for 2020–2049 and 2040–2069 (ET increase is projected by 70 % and 72 % of the simulations, respectively). Higher uncertainty was found for 2070–2096 (ET increase projected by 58 % of the simulations). ET reduction is further amplified during the summer months, where the average change of ET projected by all models is negative in all periods (up to −4.4 % in 2070–2096, Tables S4-S7).

3.4. Root zone soil moisture

The increase of ET induced by the temperature rise causes a reduction in soil moisture in the first layers (namely, in the root zone),

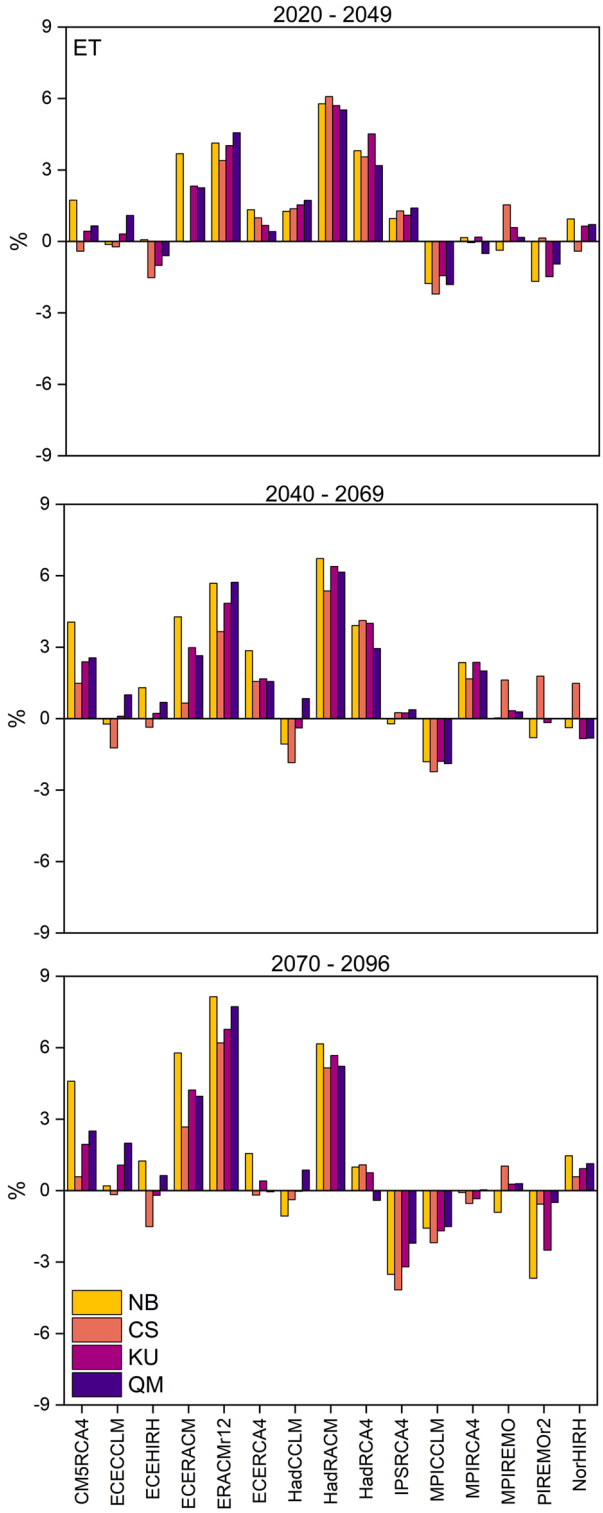

Fig. 8. Comparison between ET percentage changes achieved with the four correction methods for the 15 GCM-RCM combinations available. The top, centre and bottom rows relate to 2020–2049, 2040–2069 and 2070–2096, respectively.

even in those simulations (like HadRACM in 2020–2049) that do not project a reduction in precipitation. Fig. 9 shows for HadRACM (but the same behaviour persists for all simulations) slightly negative or even positive changes of the root zone soil moisture (RZ) during winter months due to the upper constraint given by the saturated conditions. Wet months precipitation combined with lower ET

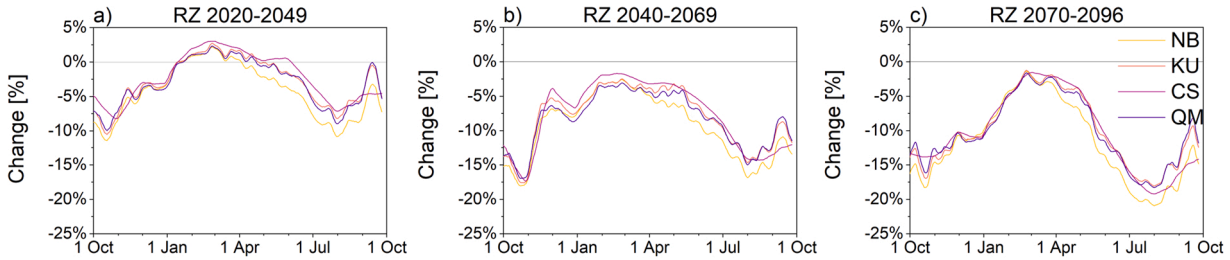

Fig. 9. Same as Fig. 5, but for root zone soil moisture RZ.

Table 5
Same as Table 3, but for yearly root zone soil moisture.

	2020–2049	2040–2069	2070–2096
NB	−5.24 (−3.46)	−6.73 (−8.36)	−9.50 (−10.51)
KU	−4.05 (−2.01)	−5.21 (−6.89)	−7.58 (−8.95)
CS	−4.10 (−1.20)	−5.49 (−6.11)	−7.89 (−8.59)
QM	−4.45 (−2.27)	−5.70 (−7.39)	−7.77 (−9.13)

values increases RZ close to saturation so that at the end of the winter, the highest values are reached anyway. Then, the increased temperature causes a more robust reduction in the warmer and drier summer months, implying yearly reductions varying from approximately 2 % (2020–2049) to 9 % (2070–2096) (Table 5). The spatial distribution of the yearly RZ generally follows that of ET (Fig. S3).

Expanding the analysis to the whole ensemble, Table 5 shows that for all periods and correction methods, average reductions are projected yearly, with overall average values of − 4.5 %, − 5.8 % and − 8.2 %, respectively, for the periods 2020–2049, 2040–2069 and 2070–2096. Slightly higher percentages are achieved for the irrigation period (Tables S8-S11). In agreement with ET outcomes, the most significant decrease is projected by NB simulations. Simulations outputs are highly consistent in projecting reduction, yearly (Fig. 10) and seasonal (Tables S8-S11).

3.5. Groundwater storage

The In-STRHyM model accounts for downward water flow from the unsaturated zone towards the saturated zone as soon as the water content in the former is higher than the field capacity. This condition occurs relatively often during wintertime, even with reduced precipitation. Fig. 11 shows that with HadRACM, winter recharge allows positive changes in the schematised unconfined aquifer depth (AQDP hereafter) at the end of the cold and wet season for 2020–2049 when precipitation increase is projected (Table 6). The behaviour is the same in the other two periods but shifted downwards (negative yearly changes in all cases). The spatial distribution of annual changes (Fig. S4) shows that the most relevant changes occur in the two latter periods in the mountain areas, while groundwater flow towards the valley reduces climate change effects.

Table 6 shows that average yearly changes are negative regardless of the period considered (overall average values equal to −2.1 %, −2.9 % and −4.3 %, respectively, for 2020–2049, 2040–2069 and 2070–2096). Similar values are achieved in the irrigation period (Tables S12-S15). Once more, the most significant decrease is projected by NB simulations, even though Fig. 12 highlights that almost all simulations agree in predicting AQDP reduction, especially in the period 2070–2096.

3.6. Runoff

In the schematisation proposed by the In-STRHyM model, surface runoff results from a saturation excess mechanism; hence it strongly depends on soil saturation and the ability of groundwater to feed the river network. Therefore, discharge (Q) changes generally resemble those achieved for RZ and AQDP and amplify them. The annual reference value of the control period simulation driven by observations is approximately 14 m^3s^{-1}. Table 7 and Fig. 13 highlight increasingly marked reductions from 2020–2049 to 2070–2096. Such as for the previous variables, the worst (most significant reduction) scenario is projected by the NB simulations. Looking at the sub-yearly time scale, on average, the seasons with the highest percentage reductions are summer (NB and KU) and spring (CS and QM) (Tables S16-S19). The flow recession phase, also due to the reduced contribution of snow melting, is mainly affected by the projected climatic change, enhancing water shortage issues in the irrigation period.

Concerning the HadRACM simulation, Table 7 and Tables S16-S19 highlight a slight increase in the first future period but a more significant reduction in the following two, compared to the average of projections. This behaviour agrees with RZ and AQDP variables for the same model.

However, in addition to the evaluation of the annual or seasonal average changes, which provide an idea of the available volumes, it is also interesting to observe the variations in the discharge values daily frequency, to verify whether a proportional change in the

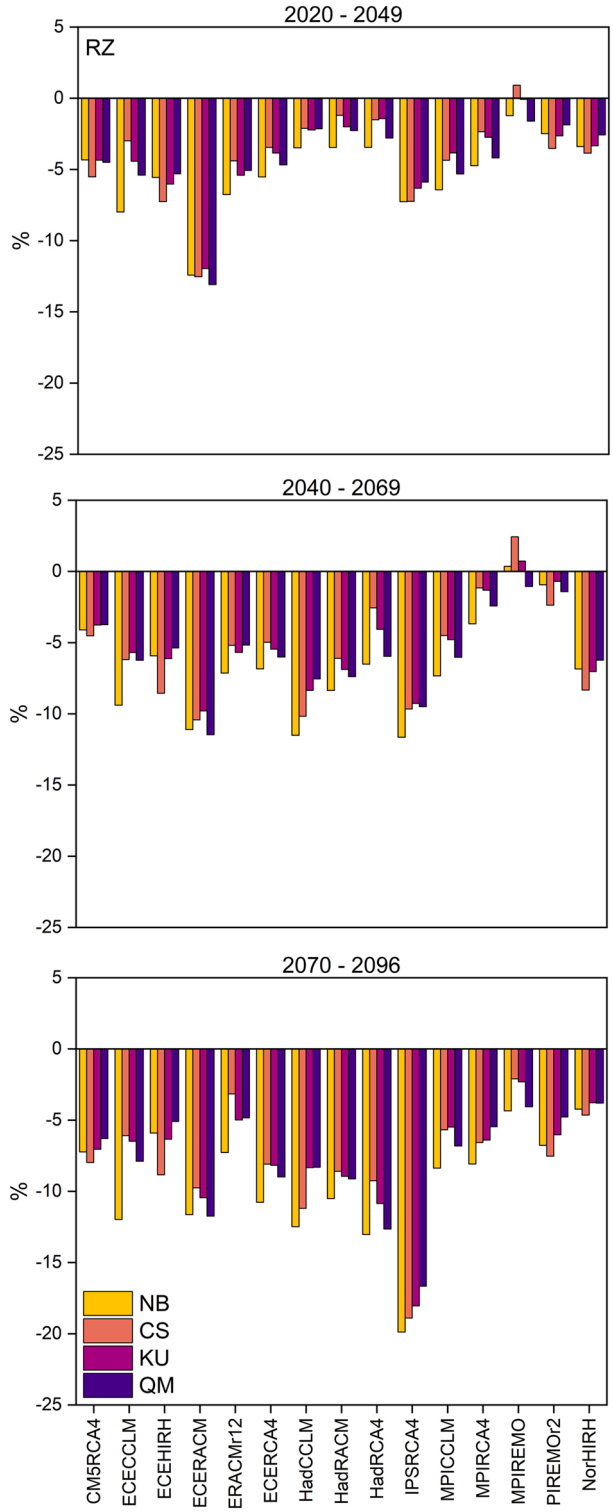

Fig. 10. Same as Fig. 8, but for RZ.

streamflow extremes (both maximum and minimum) is projected. For this purpose, the changes of some relevant flow percentiles were analysed. Flow percentile Q*n* is the daily flow equal or exceeding for *n* % of the time. Fig. 14 shows the variability of Q90 (low flow, reference value from the model driven by observations in the control period approximately equal to 0.8 m^3s^{-1}), Q50 (median flow, reference value 5.3 m^3s^{-1}) and Q10 (high flow, reference value 30 m^3s^{-1}) changes projected by the GCM-RCM combinations

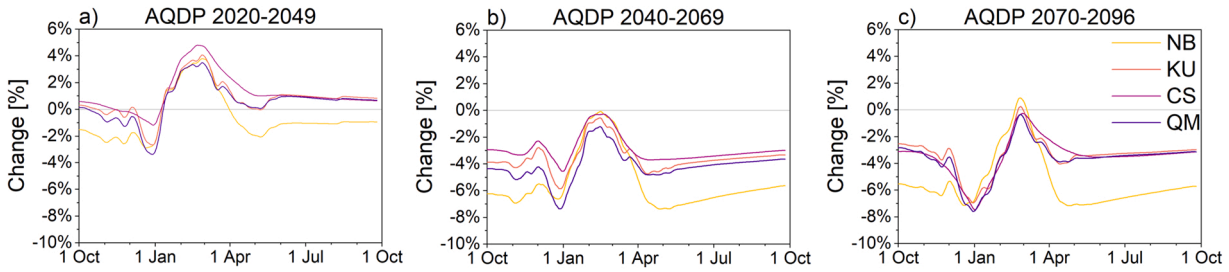

Fig. 11. Same as Fig. 5, but for the schematised unconfined aquifer depth AQDP.

Table 6
Same as Table 3, but for yearly groundwater storage.

	2020–2049	2040–2069	2070–2096
NB	−2.75 (−0.60)	−3.75 (−5.35)	−5.51 (−5.37)
KU	−1.70 (+0.87)	−2.38 (−3.53)	−3.66 (−3.34)
CS	−1.73 (+1.30)	−2.66 (−2.93)	−4.08 (−3.43)
QM	−2.12 (+0.59)	−2.91 (−4.13)	−4.10 (−3.63)

(percentage results for all models are reported in Table S20). The primary outcome is that low flows (Q90) percentage reduction is more prominent than high flow (Q10) reduction. In percentage, overall discharge decrease induced by reduced precipitation and increased temperature affects more summer low flows, due to missed wet-season recharge, than winter discharge peaks, which in turn are mainly given by isolated high precipitation events. Interestingly, in 2020–2049 the HadRACM model (black squares in Fig. 14) projects both Q90 reductions and Q10 increase with all the correction methods, indicating more extreme low and high flow events.

3.7. Sources of uncertainty

Fig. 15 shows the variance decomposition of uncertainties between GCM-RCM projections and bias correction methods for the variables ET, RZ, AQDP and Q yearly. Results highlight clearly that the GCM-RCM combinations are the primary source of uncertainty. The average value in the three future periods of the term NSS_{GR} varies from 74.8 % (with AQDP) to 81.1 % (with ET). The variance attributed to the bias correction (BC) methods NSS_{BC} is equal to 8.5 ± 3.3 % overall, while that due to interaction $NSS_{GR\times BC}$ is slightly higher (13.4 ± 1.7 %). Even though there is no clear trend among the three future periods, GCM-RCM projections are responsible for a slightly greater variance in the first one.

Next to the variance decomposition for all the available projections, an uncertainty analysis is performed, focusing only on the results achieved for bias correction methods (i.e., CS, KU and QM). Even though, theoretically, avoiding bias correction could be a reasonable option, often it is unavoidable to allow proper use of RCMs' outputs in impact assessment studies. Therefore, this further analysis allows isolating the effects of input data correction since previous results (Sections 3.2 to 3.6) highlighted the different NB projections behaviour. The results achieved excluding the option of no bias correction slightly increase the role of GCM-RCM projections. NSS_{GR} varies from 78.0 % (AQDP) to 83.5 % (Q), the variance related to BC methods decreases to 6.9 ± 1.1 % overall, while that due to interactions remains almost the same (13.3 ± 2.4 %).

As explained in Section 2.5, the large variety of GCM-RCM combinations available allows further analysis of variance decomposition focusing on GCM or RCM contribution. Fig. 16 shows the results achieved using the same GCM (i.e., ICHEC-EC-EARTH). In this case, the sources of uncertainties are the RCM, the BC methods or their interaction. Compared to the previous analysis involving both GCMs and RCMs, the contribution to uncertainty due to the different RCMs is much reduced. The average NSS_{RCM} value in the three future periods varies from 37.3 % (Q) to 72.5 % (RZ) at the yearly scale. The interaction term $NSS_{RCM\times BC}$ increases (overall average value of 30.1 ± 23.8 %), while NSS_{BC} increases less (12.5 ± 8.8 %). In particular, the variance of Q attributed exclusively to the RCMs decreases significantly, being the interaction term the greatest ($NSS_{RCM\times BC}$ almost always greater than 50 %). On the other hand, excluding NB projections from the analysis cuts back BC contribution to the variance, with NSS_{BC} reducing to 10.3 ± 7.8 % and $NSS_{RCM\times BC}$ to 22.4 ± 11.7 %.

Fig. 17 considers model combinations always using the same RCM (i.e., SMHI-RCA4), therefore highlighting the effects on the uncertainty of the GCMs only, combined with the BC methods. The results, in this case, are closer to those shown in Fig. 15. The average NSS_{GCM} value in the three future periods varies from 65.4 % (RZ) to 72.5 % (RZ). Nevertheless, the average NSS_{BC} increases, reaching not negligible values considering all the projections (overall average value of 17.3 ± 7.4 %, reduced to 10.3 ± 5.9 % if NB projections are removed from the analysis).

4. Discussion

Our discussion will first focus on comparing the results of this study with other climate change projections in the Mediterranean

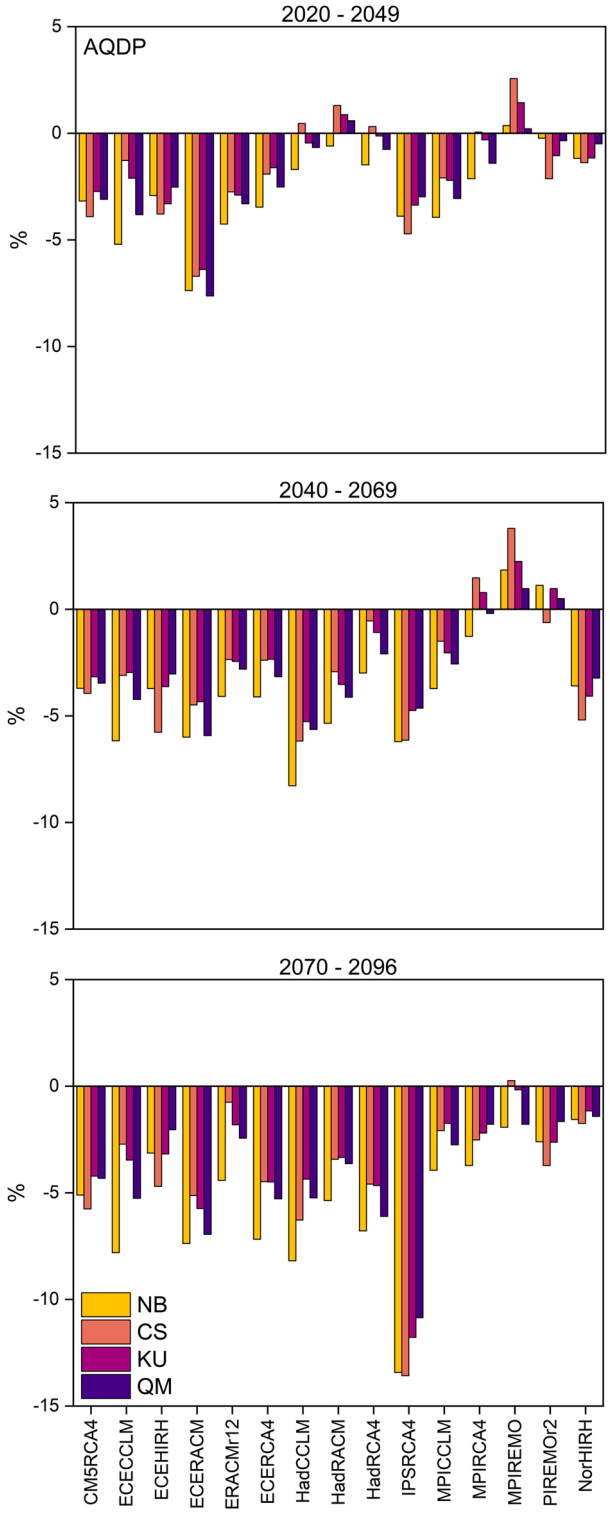

Fig. 12. Same as Fig. 8, but for AQDP.

Table 7
Same as Table 3, but for yearly discharge.

	2020–2049	2040–2069	2070–2096
NB	−9.39 (+3.02)	−14.32 (−19.87)	−19.06 (−19.56)
KU	−6.67 (+6.17)	−11.13 (−16.31)	−15.47 (−15.66)
CS	−4.87 (+12.28)	−10.42 (−12.36)	−16.59 (−14.50)
QM	−7.40 (+8.33)	−13.32 (−18.37)	−16.23 (−11.83)

area (primarily southern Italy) and then on the uncertainty analysis and the impact of different bias correction methods.

4.1. Comparison with other climate change studies

Our precipitation and temperature projections, providing less evident precipitation decrease than temperature increase, are consistent with other studies performed in the Mediterranean basin (e.g., Zittis et al., 2019, which use different CORDEX domains at a spatial resolution of 50 km). Specifically, the Mediterranean areas for which more significant rainfall reductions are expected are north-western Africa and the eastern Mediterranean. At the same time, the central-north Mediterranean lies in the borders of a kind of "transition" zone where projections are more uncertain (Tuel and Eltahir, 2020). In their previous study in the Crati River Basin, Senatore et al. (2011) considered SRES A2 and A1B scenarios comparing the future period 2070–2099 to the reference period 1961–1990. They also found a moderate decrease in cumulative yearly precipitation and a more marked temperature increase.

Concerning snow, we found reductions varying from − 50 % to − 70 % from 2020–2049 to 2070–2096, respectively (Table 3). In their previous study on the same area, Senatore et al. (2011) estimated decreases ranging from − 82 % to − 92 %. No other examples of snow projection at the catchment scale in southern Italy are available to our knowledge. Di Sante et al. (2021) project relevant snow reductions in the central and eastern Mediterranean using EURO-CORDEX, CMIP5 and CMIP6 simulations, but their analysis is at a lower resolution. Higher detail studies focusing on Spanish mountain ranges highlight reductions like those achieved in the Crati catchment. Collados-Lara et al. (2019), using RCP8.5 and considering the future period 2071–2100, found a mean reduction in the area covered by the snow of 60 % in Spanish Sierra Nevada. López-Moreno et al. (2017), using both RCPs 4.5 and 8.5, found reductions varying from 40 % to 60 % in the Sierra Nevada and the Pyrenees by 2050.

Regarding ET, we projected mean annual changes ranging from − 4.2 % (IPSRCA4, CS, 2070–2096) to + 8.1 % (ECERACMr12, NB, 2070–2096) (Tables S4-S7). Senatore et al. (2011) also found results for the period 2070–2099 that disagreed concerning the sign of the projected change at the yearly scale, with variations ranging from − 8.3 % to + 2.5 %. Nevertheless, all models projected sharp negative changes during the summer months. Perra et al. (2018), focusing on a Sardinian catchment, considering the SRES A1B emission scenario and the future period 2041–2070, generally (four of the five hydrological models used) found ET reductions (up to −12 %), especially during summertime. Pumo et al. (2016) focused their analysis on reference evapotranspiration for small catchments in Sicily and periods 2045–2065 and 2081–2100, finding percentage increments in the range from 0.35 % (RCP4.5) to 8.2 % (RCP8.5). In general, all results related to southern Italy agree in projecting an increasing inability of the actual evapotranspiration flow to match the potential demand, particularly during the summer months. This behaviour is due to drier soil conditions than the reference period.

In their projections of root zone soil moisture, Senatore et al. (2011) found an unequivocal reduction in the Crati River Basin (ranging from −13 % to −21 %), more intense than in this study (from −7.6 % to −9.5 % in 2070–2096, on average; Table 5), with not negligible reduction even in wintertime. The simulations performed by Perra et al. (2018) also showed a reduction of the soil water content at 1 m depth for the future period (approximately 9 %). On the other hand, Pumo et al. (2016) found different intensities of climate change effects in the analysed non-perennial catchments since soil hydraulic characteristics can mitigate the impact of the meteorological forcing. Finally, D'Oria et al. (2019), in their analysis concerning northern Tuscany, scenarios RCP4.5 and 8.5 and periods ranging from 2030 to 2060, highlighted that reduced soil moisture reflects not only in reduced ET but also reduced percolation.

Previous projections on groundwater storage achieved by Senatore et al. (2011) in the Crati River Basin showed reductions varying from − 7 % to − 12%. These reductions are sharper than projected in this study (from −3.7 % to −5.5 % in 2070–2096, on average; Table 6), similarly to RZ. In their study area in Tuscany, D'Oria et al. (2019) estimated percolation volume variations of − 3.3 % in 2031–2040 and − 8.1 % in 2051–2060. Pumo et al. (2016) showed that climate change effects could reduce subsurface flow contribution in small Mediterranean catchments. Another result concerning the Italian territory (even though not addressing an area with Mediterranean climate) was shown by Citrini et al. (2020), which projected ensemble mean discharges for a pre-Alpine karst spring lower than observations (3–23 %) despite the not clear trend in precipitation. Both there and in the analysed case study, even slightly increased annual precipitation cannot balance increases in evapotranspiration rates.

Finally, concerning surface runoff, projection results in agreement with previous literature highlight that the problem of water scarcity connected to low flows will be particularly emphasised. Senatore et al. (2011) projected average yearly reductions varying from − 25 % to − 41 % in the same basin (we found from −15.5 % to −19.1 % in 2070–2096, on average; Table 7). Perra et al. (2018) estimated average decreases of 31 % in their Sardinian catchment, while D'Oria et al. (2019) found for their catchment in Tuscany that the decrease in the streamflow volume is two times the precipitation decrease. Peres et al. (2019) estimated a significant reduction of future inflow in one of the most critical Sicilian reservoirs. Similar runoff reductions were projected in other northern Mediterranean regions (e.g., between 10 % and 30 % through the 21st century in Spain; Estrela et al., 2012). Such an increasing drying scenario requires adequate tools for planning (e.g., Maiolo et al., 2017) and emergency management (e.g., Mendicino and Versace, 2007). On the other hand, both the results of this study and previous projections show that, in the analysed area, it is also necessary to continue

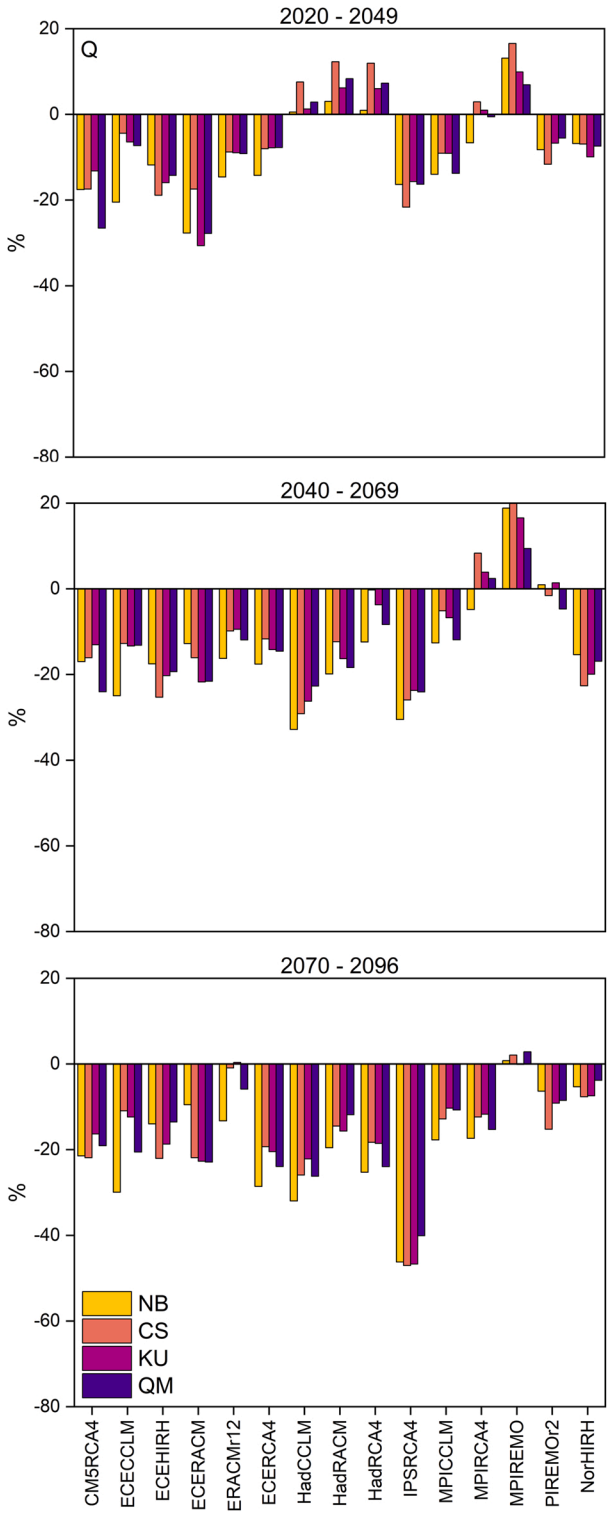

Fig. 13. Same as Fig. 8, but for the discharge at the catchment outlet Q.

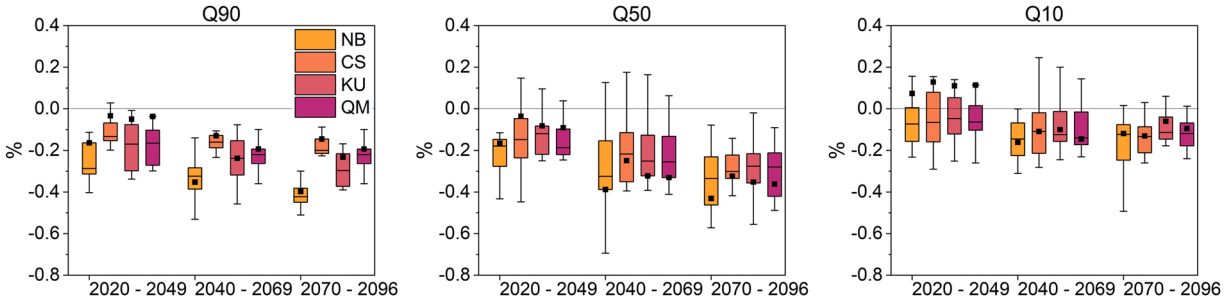

Fig. 14. Percentage changes of discharges equalled or exceeded 90 %, 50 % and 10 % of the time (Q90, Q50 and Q10, respectively) for different corrections and future periods. Q90 represents low flow, Q50 the median flow and Q10 high flow. The box and whiskers plots account for combined GCM-RCM models' variability for each bias correction method and projection period. The black squares refer to the HadRACM model.

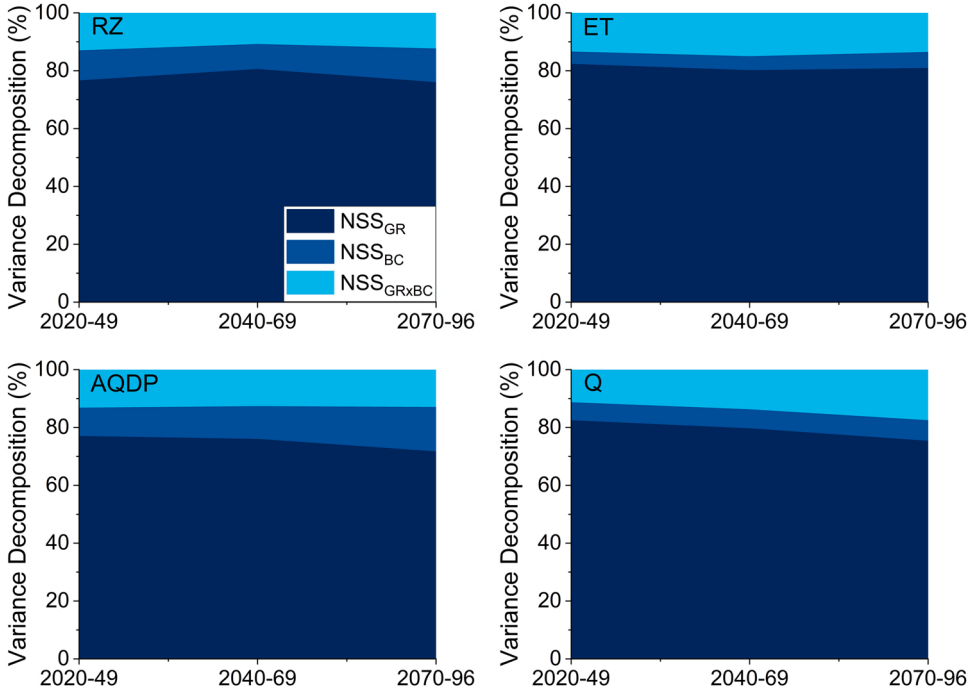

Fig. 15. Variance decomposition of the uncertainties for ET, RZ, AQDP and Q at the yearly scale. The unbiased variance fractions (*NSS*) shown are related to the combined GCM-RCM projections (NSS_{GR}), the bias correction methods (NSS_{BC}) and their interaction ($NSS_{GR\times BC}$).

keeping the flood risk under control since high flows will not decrease as much.

In general, comparison with existing literature shows that this study confirms the trends previously detected. Even though some previous sharp projections are smoothed, the overall drying scenario is the most likely.

4.2. Uncertainty analysis and impact of bias correction methods

The results achieved with the uncertainty analysis further support the assumption that the primary source is the GCM (Chen et al., 2013; Ashraf Vaghefi et al., 2019), which is responsible for approximately the 80 % of the total uncertainty. The main CCS features do not change significantly, considering the whole ensemble, whether a bias correction method is applied or not. Nevertheless, comparisons between the NB and the bias correction methods outcomes unequivocally show that bias correction reduces the projected hydrological impact of the changing climate forcing, especially on river runoff. With this variable, the average decrease of yearly discharge with NB is about 3 % higher than the average of the results achieved with the bias correction methods in every future period (Table 7). This result agrees with previous literature and can be generalised.

Limiting the analysis on RCM and BC methods (i.e., using the same GCM; Fig. 16), the uncertainties associated with these two components are more comparable, with the latter even prevailing during the irrigation period (not shown), when low flows occur. This result holds either considering or not the NB option, with the overall uncertainty attributable to the RCM varying from 57 % (including

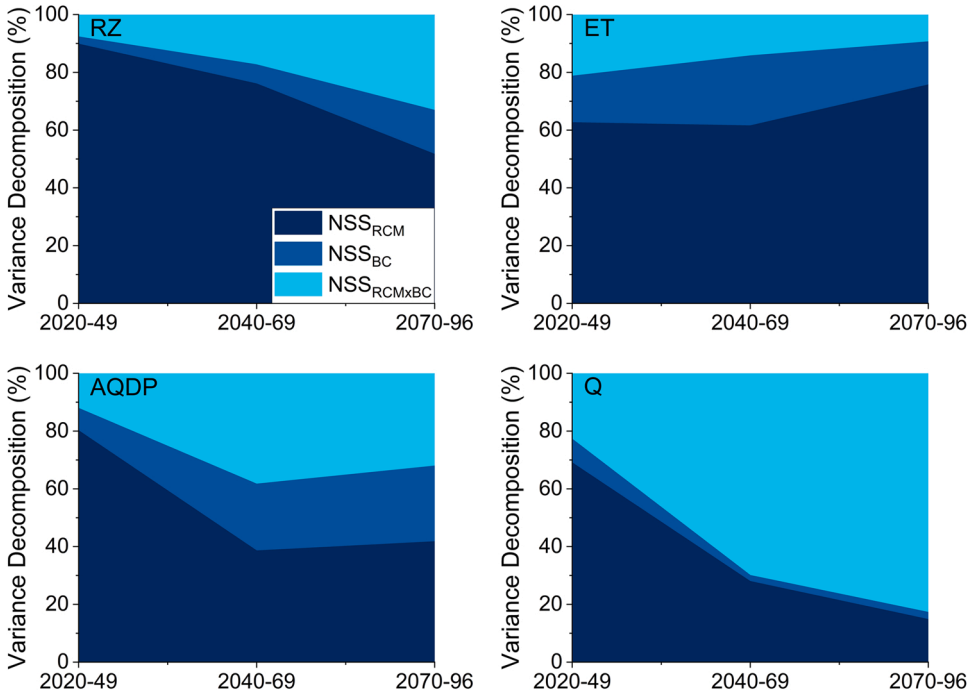

Fig. 16. Same as Fig. 15 but considering four projections sharing the same GCM (ICHEC-EC-EARTH). The four projections are ECECCLM, ECEHIRH, ECERACM and ECERCA4. *NSS* shown is related to the RCM projections (NSS_{RCM}), the bias correction methods (NSS_{BC}) and their interaction ($NSS_{RCM\times BC}$).

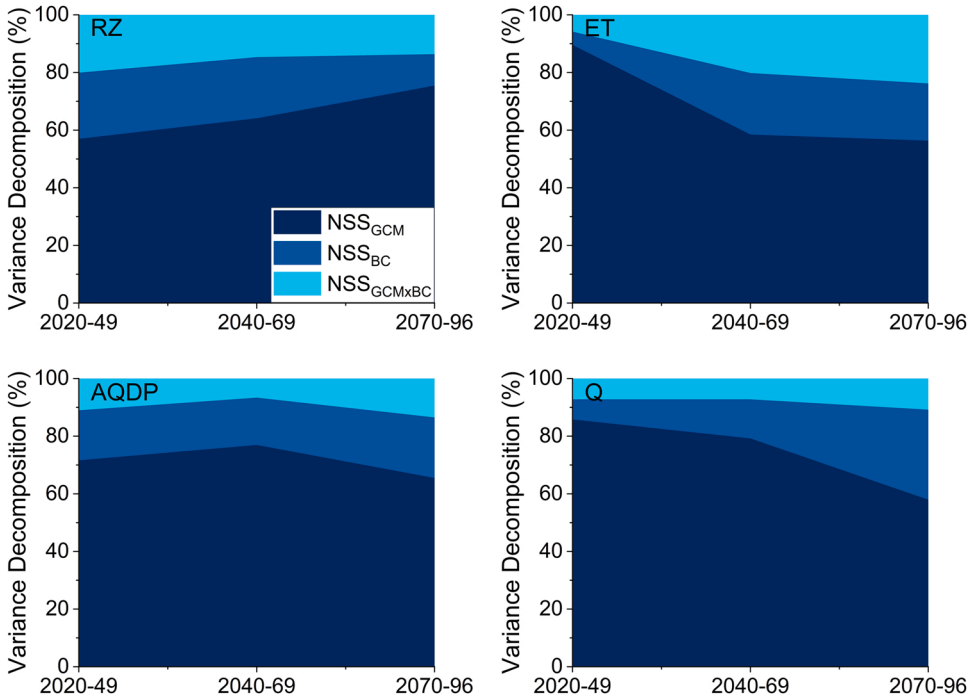

Fig. 17. Same as Fig. 15 but considering four projections sharing the same RCM (SMHI-RCA4). The four projections are CM5RCA4, ECERCA4, HadRCA4 and MPIRCA4. *NSS* shown is related to the GCM projections (NSS_{GCM}), the bias correction methods (NSS_{BC}) and their interaction ($NSS_{GCM\times BC}$).

NB in the ANOVA) to 67 % (excluding NB). In particular, the interaction term contributes to total uncertainty up to 30 % and is particularly relevant for runoff. This outcome agrees with recent studies highlighting the effects of combined climate model drivers and bias correction techniques (Aryal et al., 2019; Meresa et al., 2021) and can also be generalised.

To explain the more substantial influence of both BC-derived and BC-RCM interaction-derived uncertainty on Q, it should be considered that streamflow results from the combined effect of other processes (namely snow melting, interception, infiltration, evapotranspiration and baseflow). The In-STRHyM framework, assuming a saturation excess mechanism, follows this assumption.

The analysis performed in this study addresses only a tiny portion of the overall cascade of uncertainty concerning the projection of climate change hydrological impact. Virtually, the investigation could be extended almost indefinitely, starting from the choice of the RCP, e.g. the debated RCP8.5, which is the closest to reality for some authors (Schwalm et al., 2020), highly unlikely for others (Hausfather and Peters, 2020). Nevertheless, the detailed analysis of a given model generation becomes less critical when a new model generation with improved capabilities comes out, whereby the previously defined hierarchy of problems could be significantly changed. E.g., the new generation of CMIP6 earth system models portends improved simulations (Fernandez-Granja et al., 2021), while convection-permitting RCMs should assure higher accuracy on rainfall extremes projections (Yu et al., 2020).

5. Conclusions

In this study, we performed an uncertainty evaluation of the modelling chain to assess the climate change hydrological impact. The interested portion of the chain included the GCM-RCM combinations and bias correction methods. The exercise was demonstrated in the Crati River Basin (southern Italy). Considering the RCP4.5 scenario, 6 GCMs and 5 high-resolution (0.11°) RCMs were used in 15 combinations available through the EURO-CORDEX project. Furthermore, precipitation and temperature data derived from the RCMs and used as input for the hydrological model In-STRHyM were uncorrected and corrected using three different bias correction methods. The simulations performed considering all the available options led to 60 hydrological projections for three future periods (2020–2049, 2040–2069 and 2070–2096). Such projections allowed a detailed analysis of the projected trends of many meteo-hydrological quantities and the evaluation of the contribution of different sources to the total predicted uncertainty of the projected variables.

Concerning the amplitude and the uncertainty of the projected climate change signal, precipitation projections indicate an increasing reduction in average, even though simulations results are not unanimous. On the other hand, uncorrected projections of temperature unambiguously indicate a continuously increasing trend. Snow accumulation will reduce approximately from 50 % to 70 %, regardless of the BC method used. Actual ET will increase in the range of + 0.5 % to + 2 %, even though there is partial model disagreement (especially in the period 2070–2096). Root zone soil moisture and groundwater storage simulations unequivocally project yearly reductions (in the range of −4 % to −9.5 % and −1.5 % to −5.5 %, respectively). Finally, for runoff data, models substantially agree on mean future reduction (up to −19.1 % in 2070–2096), projecting more frequent low flows and persisting high flows.

Concerning the analysis of the relative contribution of different sources of uncertainty, the relative effect of the BC methods compared with the overall GCM-RCM modelling chain is generally small, mainly due to the great influence of the GCM choice. On the other hand, the relative effect of the BC methods compared with the RCMs only is more notable, with an increasing impact of the interactions between BC methods and RCMs. Furthermore, it is shown that applying a bias correction method to the climate forcing produces a smoothing of the projected water resources reduction, particularly concerning river runoff.

Overall, this study confirms the decreasing trend of projected water resources availability in the Crati River Basin with unprecedented detail. Furthermore, it demonstrates that: (i) multimodel approach, especially concerning GCMs, is crucial for evaluating the uncertainty of the projected hydrological impact of climate change; (ii) the BC methods do not modify the main features of the projected climate change signal substantially, but their effects are not negligible, especially when the analysis focuses on specific hydrological variables such as river runoff.

CRediT authorship contribution statement

Alfonso Senatore: Conceptualisation, Methodology, Formal analysis, Writing – original draft and review, supervision; **Domenico Fuoco:** Software, Formal analysis, Visualisation, Resources. **Mario Maiolo:** Conceptualisation, Methodology, Contribution to writing. **Giuseppe Mendicino:** Conceptualisation, Methodology, Contribution to writing. **Gerhard Smiatek:** Conceptualisation, Methodology, Resources, contribution to writing. **Harald Kunstmann:** Conceptualisation, Methodology, Contribution to writing.

Declaration of Competing Interest

The authors declare that they have no known competing financial interests or personal relationships that could have appeared to influence the work reported in this paper.

Acknowledgements

The authors thank the "Centro Funzionale Multirischi – ARPACAL" for providing the observed precipitation and temperature data. The authors also acknowledge support from the EURO-CORDEX initiative, whose climate data and projections are freely available at the EURO-CORDEX website (https://www.euro-cordex.net/). Finally, the authors thank Dr Jessica Castagna and Dr Luca Furnari for

their support with revised figures.

Appendix A. – Description of the bias correction methods

Change factor method: constant scaling

Strictly speaking, a change factor method does not correct modelled precipitation but only adjusts the observations with the modelled climate change signal (CCS). The adjusted (*adj* subscript) daily (*d*) precipitation values in the future (*fut*) scenario $P_{adj,fut,d}$ are calculated for each cell of the computational domain starting from the observed series. In particular, each observed (*obs*) daily precipitation value $P_{obs,d}$ is multiplied by the ratio between the average precipitation projected by the RCM in month m to which day d belongs $\overline{P}_{RCM,fut,m}$ and the average rainfall modelled in the control period (*ref* subscript, 1975–2005 in our case) in the same month $\overline{P}_{RCM,ref,m}$:

$$P_{adj,fut,d} = P_{obs,d} \times \left(\overline{P}_{RCM,fut,m} / \overline{P}_{RCM,ref,m}\right) \tag{A.1}$$

Conversely, adjusted daily temperature values in the future scenario $T_{adj,fut,d}$ are calculated for each cell, adding to the observed daily values $T_{obs,d}$ the difference between the average temperature projected by the RCM in month m to which day d belongs $\overline{T}_{RCM,fut,m}$ and the average temperature modelled in the control period in the same month $\overline{T}_{RCM,ref,m}$:

$$T_{adj,fut,d} = T_{obs,d} + \left(\overline{T}_{RCM,fut,m} - \overline{T}_{RCM,ref,m}\right) \tag{A.2}$$

Scaling bias correction approach

This bias correction method, proposed by Kunstmann et al. (2004), is important in this research because it was adopted in the previous study on the hydrological impact of climate change over the Crati River Basin (Senatore et al., 2011). Therefore, it can provide valuable insights into comparing old and new projections.

With the KU method, historical and future RCMs daily d precipitation ($P_{RCM,ref,d}$ and $P_{RCM,fut,d}$, respectively) and temperature ($T_{RCM,ref,d}$ and $T_{RCM,fut,d}$, respectively) are modified through a monthly correction parameter K depending on both modelled and observed variables. As for precipitation P, each monthly m correction parameter $K_{P,m}$ is calculated cell by cell with the following equation:

$$K_{P,m} = \frac{\sum_{year=1975}^{2005} \sum_{day=1}^{28,29,30,31} P_{RCM,ref,d,y}}{\sum_{year=1975}^{2005} \sum_{day=1}^{28,29,30,31} P_{obs,d,y}} \tag{A.3}$$

Analogously to the CS method, for the cell-by-cell calculation of the temperature monthly correction parameter $K_{T,m}$ a difference replaces the ratio between modelled and observed variables:

$$K_{T,m} = \sum_{year=1975}^{2005} \sum_{day=1}^{28,29,30,31} T_{obs,d,y} - \sum_{year=1975}^{2005} \sum_{day=1}^{28,29,30,31} T_{RCM,ref,d,y} \tag{A.4}$$

Once the precipitation and temperature correction parameters are found, they can be applied both on the control period 1975–2005 and the future period 2020–2096, multiplying (adding) them by (to) the original daily precipitation (temperature) series.

Non-parametric quantile mapping approach

With this method, the projected daily precipitation value $P_{RCM,fut,d}$ is changed according to the correction of the daily precipitation distribution calculated through empirical cumulative distribution functions (ecdfs). As a first step, the ecdfs of both the observed and simulated daily precipitation in the reference period ($ecdf_{obs,d}$ and $ecdf_{RCM,ref,d}$, respectively) are determined (including dry days). Specifically, the related probabilities of non-exceedance $Pr_{obs,d}$ and $Pr_{RCM,ref,d}$ can be obtained:

$$Pr_{obs,d} = ecdf_{obs,d}\left(P_{obs,d}\right) \tag{A.5}$$

$$Pr_{RCM,ref,d} = ecdf_{RCM,ref,d}\left(P_{RCM,ref,d}\right) \tag{A.6}$$

Correction functions *CFs* are given by the difference between observed and modelled values calculated as inverse ecdfs at the probability $Pr_{RCM,ref,d}$:

$$CF_{RCM,ref,d} = ecdf^{-1}_{obs,d}\left(Pr_{RCM,ref,d}\right) - ecdf^{-1}_{RCM,ref,d}\left(Pr_{RCM,ref,d}\right) \tag{A.7}$$

Finally, the corrected daily future precipitation values $P_{cor,fut,d}$ are provided, adding the correction functions to $P_{RCM,fut,d}$:

$$P_{cor,fut,d} = P_{RCM,fut,d} + CF_{RCM,ref,d} \tag{A.8}$$

Further details about this method are provided by Themeßl et al., (2011, 2012) and Chen et al. (2013). Theoretically, *CFs* can be calculated for each cell of the domain. However, since the basin under study is relatively small and the daily precipitation series in each

domain cell are highly correlated, the computational effort is reduced by calculating the correction coefficients based on the daily observed and simulated precipitation averaged in the whole contributing area. Further simplification concerns daily temperature data, whose future projections are largely beyond the range of the reference period. Though the original QM method (Themeßl et al., 2011, 2012) allows temperature corrections, extrapolating corrected values in these conditions would require the definition of theoretical distributions (Chen et al., 2013) with related problems concerning the fitting process and a substantial loss of information compared to empirical distributions. Therefore, in this study, the corrected temperature combined with the QM-corrected precipitation for hydrological simulations is achieved with the KU method.

Appendix B. Supporting information

Supplementary data associated with this article can be found in the online version at doi:10.1016/j.ejrh.2022.101120. These data include Google maps of the most important areas described in this article.

References

Al Aamery, N., Fox, J.F., Snyder, M., 2016. Evaluation of climate modeling factors impacting the variance of streamflow. J. Hydrol. 542, 125–142.

Allen, R., Pereira, L.S., Raes, D., Smith, M., 1998. Crop Evapotranspiration -Guidelines for Computing Crop Water Requirements. FAO Irrigation and Drainage Paper no 56, FAO, Rome.

Aryal, A., Shrestha, S., Babel, M.S., 2019. Quantifying the sources of uncertainty in an ensemble of hydrological climate-impact projections. Theor. Appl. Climatol. 135 (1–2), 193–209.

Ashraf Vaghefi, S., Iravani, M., Sauchyn, D., et al., 2019. Regionalisation and parameterisation of a hydrologic model significantly affect the cascade of uncertainty in climate-impact projections. Clim. Dyn. 53 (5), 2861–2886.

Baldauf, M., Seifert, A., Förstner, J., Majewski, D., Raschendorfer, M., Reinhardt, T., Baldauf, M., Seifert, A., Förstner, J., Majewski, D., Raschendorfer, M., Reinhardt, T., 2011. Operational Convective-Scale Numerical Weather Prediction with the COSMO Model: Description and Sensitivities. Mon. Weather Rev. 139, 3887–3905. https://doi.org/10.1175/MWR-D-10-05013.1.

Bentsen, M., Bethke, I., Debernard, J.B., Iversen, T., Kirkevåg, A., Seland, Ø., Drange, H., Roelandt, C., Seierstad, I.A., Hoose, C., Kristjánsson, J.E., 2013. The Norwegian Earth System Model, NorESM1-M – Part 1: Description and basic evaluation of the physical climate. Geosci. Model Dev. 6, 687–720. https://doi.org/10.5194/gmd-6-687-2013.

Beyene, T., Lettenmaier, D.P., Kabat, P., 2010. Hydrologic impacts of climate change on the Nile River Basin: implications of the 2007 IPCC scenarios. Clim. Change 100 (3), 433–461.

Bosshard, T., Carambia, M., Goergen, K., Kotlarski, S., Krahe, P., Zappa, M., Schär, C., 2013. Quantifying uncertainty sources in an ensemble of hydrological climate-impact projections. Water Resour. Res. 49, 1523–1536.

Bucak, T., Trolle, D., Andersen, et al., 2017. Future water availability in the largest freshwater Mediterranean lake is at great risk as evidenced from simulations with the SWAT model. Sci. Total Environ. 581, 413–425.

Cannon, A.J., Sobie, S.R., Murdock, T.Q., 2015. Bias correction of GCM precipitation by quantile mapping: How well do methods preserve changes in quantiles and extremes? J. Clim. 28 (17), 6938–6959.

Chen, J., Brissette, F.P., Leconte, R., 2011. Uncertainty of downscaling method in quantifying the impact of climate change on hydrology. J. Hydrol. 401, 190–202.

Chen, J., Brissette, F.P., Chaumont, D., et al., 2013. Performance and uncertainty evaluation of empirical downscaling methods in quantifying the climate change impacts on hydrology over two North American river basins. J. Hydrol. 479, 200–214.

Chen, J., Brissette, F.P., Lucas-Picher, P., 2015. Assessing the limits of bias-correcting climate model outputs for climate change impact studies. J. Geophys. Res. Atmos. 120, 1123–1136.

Christensen, O.B., Drews, M., Christensen, J.H., Dethloff, K., Ketelsen, K., Hebestadt, I., Rinke, A., 2007. The HIRHAM Regional Climate Model Version 5 (beta). Tech. Rep. 06-17 (5), 1–22.

Citrini, A., Camera, C., Beretta, G.P., 2020. Nossana spring (northern Italy) under climate change: Projections of future discharge rates and water availability. Water 12 (2), 387.

Collins, W.J., Bellouin, N., Doutriaux-Boucher, M., Gedney, N., Halloran, P., Hinton, T., Hughes, J., Jones, C.D., Joshi, M., Liddicoat, S., Martin, G., O'Connor, F., Rae, J., Senior, C., Sitch, S., Totterdell, I., Wiltshire, A., Woodward, S., 2011. Development and evaluation of an Earth-System model – HadGEM2. Geosci. Model Dev. 4, 1051–1075. https://doi.org/10.5194/gmd-4-1051-2011.

Collados-Lara, A.J., Pardo-Igúzquiza, E., Pulido-Velazquez, D., 2019. A distributed cellular automata model to simulate potential future impacts of climate change on snow cover area. Adv. Water Resour. 124, 106–119.

Cook, B.I., Smerdon, J.E., Seager, R., Cloats, S., 2014. Global warming and 21st century drying. Clim. Dyn. 43, 2607–2627.

Cramer, W., Guiot, J., Fader, M., et al., 2018. Climate change and interconnected risks to sustainable development in the Mediterranean. Nat. Clim. Change 8, 972–980.

Dayon, G., Boe, J., Martin, E., et al., 2018. Impacts of climate change on the hydrological cycle over France and associated uncertainties. C. R. Geosci. 350 (4), 141–153.

Di Sante, F., Coppola, E., Giorgi, F., 2021. Projections of river floods in Europe using EURO-CORDEX, CMIP5 and CMIP6 simulations. Int. J. Climatol. 41 (5), 3203–3221.

Dobler, C., Hagemann, S., Wilby, R.L., et al., 2012. Quantifying different sources of uncertainty in hydrological projections in an Alpine watershed. Hydrol. Earth Syst. Sci. 16, 4343–4360.

D'Oria, M., Ferraresi, M., Tanda, M.G., 2019. Quantifying the impacts of climate change on water resources in northern Tuscany, Italy, using high-resolution regional projections. Hydrol. Process. 33, 978–993.

Dufresne, J.-L., Foujols, M.-A., Denvil, S., Caubel, A., Marti, O., Aumont, O., Balkanski, Y., Bekki, S., Bellenger, H., Benshila, R., Bony, S., Bopp, L., Braconnot, P., Brockmann, P., Cadule, P., Cheruy, F., Codron, F., Cozic, A., Cugnet, D., de Noblet, N., Duvel, J.-P., Ethé, C., Fairhead, L., Fichefet, T., Flavoni, S., Friedlingstein, P., Grandpeix, J.-Y., Guez, L., Guilyardi, E., Hauglustaine, D., Hourdin, F., Idelkadi, A., Ghattas, J., Joussaume, S., Kageyama, M., Krinner, G., Labetoulle, S., Lahellec, A., Lefebvre, M.-P., Lefevre, F., Levy, C., Li, Z.X., Lloyd, J., Lott, F., Madec, G., Mancip, M., Marchand, M., Masson, S., Meurdesoif, Y., Mignot, J., Musat, I., Parouty, S., Polcher, J., Rio, C., Schulz, M., Swingedouw, D., Szopa, S., Talandier, C., Terray, P., Viovy, N., Vuichard, N., 2013. Climate change projections using the IPSL-CM5 Earth System Model: from CMIP3 to CMIP5. Clim. Dynam. 40, 2123–2165. https://doi.org/10.1007/s00382-012-1636-1.

Ehret, U., Zehe, E., Wulfmeyer, V., et al., 2012. HESS opinions "should we apply bias correction to global and regional climate model data?". Hydrol. Earth Syst. Sci. 16, 3391–3404.

Estrela, T., Pérez-Martin, M.A., Vargas, E., 2012. Impacts of climate change on water resources in Spain. Hydrol. Sci. J. 57 (6), 1154–1167.

Fang, G.H., Yang, J., Chen, Y.N., Zammit, C., 2015. Comparing bias correction methods in downscaling meteorological variables for a hydrologic impact study in an arid area in China. Hydrol. Earth Syst. Sci. 19, 2547–2559.

FAO, 2016. The State of Food and Agriculture: Climate Change, Agriculture and Food Security. FAO, Rome.
Fernandez-Granja, J.A., Casanueva, A., Bedia, J., et al., 2021. Improved atmospheric circulation over Europe by the new generation of CMIP6 earth system models. Clim. Dyn. 56 (11), 3527–3540.
Gampe, D., Schmid, J., Ludwig, R., 2019. Impact of reference dataset selection on RCM evaluation, bias correction, and resulting climate change signals of precipitation. J. Hydrometeorol. 20 (9), 1813–1828.
Garrote, L., Iglesias, A., Granados, A., et al., 2015. Quantitative assessment of climate change vulnerability of irrigation demands in Mediterranean Europe. Water Resour. Manag. 29, 325–338.
Giorgetta, M.A., Jungclaus, J., Reick, C.H., Legutke, S., Bader, J., Böttinger, M., Brovkin, V., Crueger, T., Esch, M., Fieg, K., Glushak, K., Gayler, V., Haak, H., Hollweg, H.-D., Ilyina, T., Kinne, S., Kornblueh, L., Matei, D., Mauritsen, T., Mikolajewicz, U., Mueller, W., Notz, D., Pithan, F., Raddatz, T., Rast, S., Redler, R., Roeckner, E., Schmidt, H., Schnur, R., Segschneider, J., Six, K.D., Stockhause, M., Timmreck, C., Wegner, J., Widmann, H., Wieners, K.-H., Claussen, M., Marotzke, J., Stevens, B., 2013. Climate and carbon cycle changes from 1850 to 2100 in MPI-ESM simulations for the Coupled Model Intercomparison Project phase 5. J. Adv. Model. Earth Sy. 5, 572–597. https://doi.org/10.1002/jame.20038.
Giorgi, F., Gutowski Jr., W.J., 2015. Regional dynamical downscaling and the CORDEX initiative. Annu. Rev. Environ. Resour. 40 (1), 467–490.
Giorgi, F., Lionello, P., 2008. Climate change projections for the Mediterranean region. Glob. Planet. Change 63 (2–3), 90–104.
Giorgi, F., Jones, C., Asrar, G.R., 2009. Addressing climate information needs at the regional level: the CORDEX framework. WMO Bull. 58 (3), 175.
Gobiet, A., Kotlarski, S., Beniston, et al., 2014. 21st century climate change in the European Alps—a review. Sci. Total Environ. 493, 1138–1151.
Gorguner, M., Kavvas, M.L., Ishida, K., 2019. Assessing the impacts of future climate change on the hydroclimatology of the Gediz Basin in Turkey by using dynamically downscaled CMIP5 projections. Sci. Total Environ. 648, 481–499.
Gudmundsson, L., Seneviratne, S., Zhang, X., 2017. Anthropogenic climate change detected in European renewable freshwater resources. Nat. Clim. Change 7, 813–816.
Gutmann, E.D., Rasmussen, R.M., Liu, C., et al., 2012. A comparison of statistical and dynamical downscaling of winter precipitation over complex terrain. J. Clim. 25 (1), 262–281.
Hazeleger, W., Severijns, C., Semmler, T., Ştefănescu, S., Yang, S., Wang, X., Wyser, K., Dutra, E., Baldasano, J.M., Bintanja, R., Bougeault, P., Caballero, R., Ekman, A. M.L., Christensen, J.H., van den Hurk, B., Jimenez, P., Jones, C., Kållberg, P., Koenigk, T., McGrath, R., Miranda, P., van Noije, T., Palmer, T., Parodi, J.A., Schmith, T., Selten, F., Storelvmo, T., Sterl, A., Tapamo, H., Vancoppenolle, M., Viterbo, P., Willén, U., 2010. EC-Earth. B. Am. Meteorol. Soc. 91, 1357–1364. https://doi.org/10.1175/2010BAMS2877.1.
Hadour, A., Mahé, G., Meddi, M., 2020. Watershed based hydrological evolution under climate change effect: an example from North Western Algeria. J. Hydrol. Reg. Stud. 28, 100671.
Hartmann, A., Gleeson, T., Wada, Y., et al., 2017. Enhanced groundwater recharge rates and altered recharge sensitivity to climate variability through subsurface heterogeneity. PNAS 114 (11), 2842–2847.
Hausfather, Z., Peters, G.P., 2020. Emissions – the 'Business as Usual' Story Is Misleading. Nature 577, 618–620.
Hertig, E., Tramblay, Y., 2016. Regional downscaling of Mediterranean droughts under past and future climatic conditions. Glob. Planet. Change 151, 36–48.
Ho, C.K., Stephenson, D.B., Collins, M., Ferro, C.A.T., Brown, S.J., 2012. Calibration strategies: a source of additional uncertainty in climate change projections. Bull. Am. Meteorol. Soc. 93 (1), 21–26.
Hoegh-Guldberg, O., Jacob, D., Bindi, et al., 2018. Impacts of 1.5°C Global Warming on Natural and Human Systems, in: Masson-Delmotte V., Zhai P., Pörtner H. O., (Eds.), Global warming of 1.5°C. An IPCC Special Report, 175–311.
Huang, S., Krysanova, V., Hattermann, F.F., 2014. Does bias correction increase reliability of flood projections under climate change? a case study of large rivers in Germany. Int J. Clim. 34, 3780–3800.
Iversen, T., Bentsen, M., Bethke, I., Debernard, J.B., Kirkevåg, A., Seland, Ø., Drange, H., Kristjansson, J.E., Medhaug, I., Sand, M., Seierstad, I.A., 2013. The Norwegian Earth System Model, NorESM1-M – Part 2: Climate response and scenario projections. Geosci. Model Dev. 6, 389–415. https://doi.org/10.5194/gmd-6-389-2013.
IPCC, 2014. Climate Change 2014: Synthesis Report. Contribution of Working Groups I, II and III to the Fifth Assessment Report of the Intergovernmental Panel on Climate Change [Core Writing Team, R.K. Pachauri and L.A. Meyer (eds.)]. IPCC, Geneva, Switzerland, 151 pp.
Jacob, D., Petersen, J., Eggert, B., et al., 2014. EURO-CORDEX: new high-resolution climate change projections for European impact research. Reg. Environ. Change 14 (2), 563–578.
Johnson, F., Sharma, A., 2015. What are the impacts of bias correction on future drought projections? J. Hydrol. 525, 472–485.
Kim, K.B., Kwon, H.H., Han, D., 2015. Bias correction methods for regional climate model simulations considering the distributional parametric uncertainty underlying the observations. J. Hydrol. 530, 568–579.
Koutroulis, A.G., Tsanis, I.K., Daliakopoulos, I.N., et al., 2013. Impact of climate change on water resources status: a case study for Crete Island. Greece J. Hydrol. 479, 146–158.
Kriestensen, K.J., Jensen, S.E., 1975. A model for estimating actual evapotranspiration from potential evapotranspiration. Nord. Hydrol. 6, 70–88.
Kunstmann, H., Schneider, K., Forkel, R., et al., 2004. Impact analysis of climate change for an alpine catchment using high resolution dynamic downscaling of ECHAM4 time slices. Hydrol. Earth Syst. Sci. 8, 1031–1045.
Lafaysse, M., Hingray, B., Mezghani, A., et al., 2014. Internal variability and model uncertainty components in future hydrometeorological projections: The Alpine Durance basin. Water Resour. Res. 50 (4), 3317–3341.
Lee, M.-H., Qiu, L., Ha, S., Im, E.-S., Bae, D.-H., 2022. Future projection of low flows in the Chungju basin, Korea and their uncertainty decomposition. Int. J. Climatol. 42 (1), 157–174.
Li, L., Shen, M., Hou, Y., Li, J., Chen, H., 2019. Twenty-first-century glacio-hydrological changes in the Himalayan headwater Beas River basin. Hydrol. Earth Syst. Sci. 23 (3), 1483–1503.
López-Moreno, J.I., Gascoin, S., Herrero, J., et al., 2017. Different sensitivities of snowpacks to warming in Mediterranean climate mountain areas. Environ. Res. Lett. 12 (7), 074006.
Madsen, H., Lawrence, D., Lang, M., et al., 2014. Review of trend analysis and climate change projections of extreme precipitation and floods in Europe. J. Hydrol. 519 (Part D), 3634–3650.
Maiolo, M., Mendicino, G., Pantusa, D., Senatore, A., 2017. Optimisation of drinking water distribution systems in relation to the effects of climate change. Water 9 (10), 803.
Majone, B., Bovolo, C.I., Bellin, A., et al., 2012. Modeling the impacts of future climate change on water resources for the Gàllego river basin (Spain). Water Resour. Res. 48, W01512.
Majone, B., Villa, F., Deidda, R., et al., 2016. Impact of climate change and water use policies on hydropower potential in the south-eastern Alpine region. Sci. Total Environ. 543, 965–980.
Maraun, D., 2013. Bias correction, quantile mapping, and downscaling: revisiting the inflation issue. J. Clim. 26 (6), 2137–2143.
Maraun, D., Wetterhall, F., Ireson, A.M., et al., 2010. Precipitation downscaling under climate change: Recent developments to bridge the gap between dynamical models and the end user. Rev. Geophys. 48, RG3003.
Maraun, D., Shepherd, T., Widmann, M., et al., 2017. Towards process-informed bias correction of climate change simulations. Nat. Clim. Change 7, 764–773.
Mascaro, G., Viola, F., Deidda, R., 2018. Evaluation of precipitation from EURO-CORDEX regional climate simulations in a small-scale Mediterranean site. J. Geophys. Res. Atmos. 123 (3), 1604–1625.
Mendicino, G., Versace, P., 2007. Integrated drought watch system: a case study in Southern Italy. Water Resour. Manag. 21, 1409–1428.
Meresa, H., Murphy, C., Fealy, R., Golian, S., 2021. Uncertainties and their interaction in flood hazard assessment with climate change. Hydrol. Earth Syst. Sci. 25 (9), 5237–5257.
Moore, I.D., Norton, T.W., Williams, J.E., 1993. Modelling environmental heterogeneity in forested landscapes. J. Hydrol. 150, 717–747.

Mpelasoka, F.S., Chiew, F.H.S., 2009. Influence of rainfall scenario construction methods on runoff projections. J. Hydrometeorol. 10, 1168–1183.
Muerth, M.J., Gauvin St-Denis, B., Ricard, S., et al., 2013. On the need for bias correction in regional climate scenarios to assess climate change impacts on river runoff. Hydrol. Earth Syst. Sci. 17, 1189–1204.
Nakícenovíc, N., Alcamo, J., Davis, G., et al., 2000. Special Report on Emissions Scenarios. Cambridge University Press,, Cambridge.
Neitsch, S.L., Arnold, J.G., Kiniry, J.R., Williams, J.R., King, K.W., 2002. Soil and Water Assessment Tool Theoretical Documentation, Version 2000. Grassland, Soil and Water Research Laboratory – Agricultural Research Service & Blackland Research Center – Texas Agricultural Experiment Station, Temple, Texas, pp. 58–65.
Nerantzaki, S.D., Hristopulos, D.T., Nikolaidis, N.P., 2020. Estimation of the uncertainty of hydrologic predictions in a karstic Mediterranean watershed. Sci. Total Environ. 717, 137131.
Ngai, S.T., Tangang, F., Juneng, L., 2017. Bias correction of global and regional simulated daily precipitation and surface mean temperature over Southeast Asia using quantile mapping method. Glob. Planet. Chang 149, 79–90.
Olmos Giménez, P., Garcia Galiano, S., Giraldo-Osorio, J.D., 2016. Identifying a robust method to build RCMs ensemble as climate forcing for hydrological impact models. Atmos. Res. 174, 31–40.
Peres, D.J., Modica, R., Cancelliere, A., 2019. Assessing future impacts of climate change on water supply system performance: application to the pozzillo reservoir in Sicily, Italy. Water 11, 2531.
Peres, D.J., Senatore, A., Nanni, P., Cancelliere, A., Mendicino, G., Bonaccorso, B., 2020. Towards a reliable assessment of climate change impact on droughts in Southern Italy: Evaluation of EURO-CORDEX historical simulations by high-quality observational datasets. Nat. Hazards Earth Syst. 20 (11), 3057–3082.
Perra, E., Piras, M., Deidda, R., et al., 2018. Multimodel assessment of climate change-induced hydrologic impacts for a Mediterranean catchment. Hydrol. Earth Syst. Sci. 22 (7), 4125–4143.
Potter, N.J., Chiew, F.H.S., Charles, S.P., Fu, G., Zheng, H., Zhang, L., 2020. Bias in dynamically downscaled rainfall characteristics for hydroclimatic projections. Hydrol. Earth Syst. Sci. 24, 2963–2979.
Prats, J., Salencon, M.J., Gant, M., et al., 2018. Simulation of the hydrodynamic behaviour of a Mediterranean reservoir under different climate change and management scenarios. J. Limnol. 77, 62–81.
Priestley, C.H.B., Taylor, R.J., 1972. On the assessment of the surface heat flux and evaporation using large-scale parameters. Mon. Weather Rev. 100, 81–92.
Pumo, D., Caracciolo, D., Viola, F., et al., 2016. Climate change effects on the hydrological regime of small non-perennial river basins. Sci. Total Environ. 542, 76–92.
Ravazzani, G., Barbero, S., Salandin, A., et al., 2015. An integrated hydrological model for assessing climate change impacts on water resources of the upper Po River Basin. Water Resour. Manag. 29, 1193–1215.
Ronco, P., Zennaro, F., Torresan, S., et al., 2017. A risk assessment framework for irrigated agriculture under climate change. Adv. Water Resour. 110, 562–578.
Rockel, B., Will, A., Hense, A., 2008. The Regional Climate Model COSMO-CLM (CCLM). Meteorol. Z. 17, 347–348. https://doi.org/10.1127/0941-2948/2008/0309.
Schwalm, C.R., Glendon, S., Duffy, P.B., 2020. RCP8.5 tracks cumulative CO_2 emissions. PNAS 117 (33), 19656–19657.
Seaby, L.P., Refsgaard, J.C., Sonnenborg, T.O., et al., 2015. Spatial uncertainty in bias corrected climate change projections and hydrogeological impacts. Hydrol. Process. 29 (20), 4514–4532.
Sellami, H., Benabdallah, S., La Jeunesse, I., et al., 2016. Quantifying hydrological responses of small Mediterranean catchments under climate change projections. Sci. Total Environ. 543, 924–936.
Senatore, A., Mendicino, G., Smiatek, G., et al., 2011. Regional climate change projections and hydrological impact analysis for a Mediterranean basin in Southern Italy. J. Hydrol. 399 (1–2), 70–92.
Senatore, A., Hejabi, S., Mendicino, G., Bazrafshan, J., Irannejad, P., 2019. Climate conditions and drought assessment with the Palmer Drought Severity Index in Iran: evaluation of CORDEX South Asia climate projections (2070–2099). Clim. Dyn. 52 (1–2), 865–891.
Smiatek, G., Kunstmann, H., Heckl, A., 2014. High-resolution climate change impact analysis on expected future water availability in the Upper Jordan catchment and the Middle East. J. Hydrometeorol. 15 (4), 1517–1531.
Strandberg, G., Bärring, L., Hansson, U., Jansson, C., Jones, C., Kjellström, E., Kolax, M., Kupiainen, M., Nikulin, G., Samuelsson, P., Ullerstig, A., and Wang, S.: CORDEX scenarios for Europe from the Rossby Centre regional climate model RCA4, Report meteorology and climatology No. 116, Swedish Meteorological and Hydrological Institute (SMHI), ISSN: 0347-2116, 2014.
Teichmann, C., Eggert, B., Elizalde, A., Haensler, A., Jacob, D., Kumar, P., Moseley, C., Pfeifer, S., Rechid, D., Remedio, A.R., Ries, H., Petersen, J., Preuschmann, S., Raub, T., Saeed, F., Sieck, K., Weber, T., 2013. How does a regional climate model modify the projected climate change signal of the driving GCM: A study over different CORDEX regions using REMO. Atmosphere 4, 214–236. https://doi.org/10.3390/atmos4020214.
Taïbi, S., Meddi, M., Mahé, G., 2019. Seasonal rainfall variability in the southern Mediterranean border: observations, regional model simulations and future climate projections. Atmósfera 32 (1), 39–54.
Taylor, K.E., Stouffer, R.J., Meehl, G.A., 2012. An overview of CMIP5 and the experiment design. Bull. Am. Meteorol. Soc. 93, 485–498.
Teng, J., Potter, N.J., Chiew, F.H.S., et al., 2015. How does bias correction of regional climate model precipitation affect modelled runoff? Hydrol. Earth Syst. Sci. 19, 711–728.
Teutschbein, C., Seibert, J., 2013. Is bias correction of regional climate model (RCM) simulations possible for non-stationary conditions? Hydrol. Earth Syst. Sci. 17, 5061–5077.
Themeßl, M.J., Gobiet, A., Leuprecht, A., 2011. Empirical-statistical downscaling and error correction of daily precipitation from regional climate models. I. J. Clim. 31 (10), 1530–1544.
Themeßl, M.J., Gobiet, A., Heinrich, G., 2012. Empirical-statistical downscaling and error correction of regional climate models and its impact on the climate change signal. Clim. Change 112 (2), 449–468.
Tigkas, D., Vangelis, H., Tsakiris, G., 2012. Drought and climatic change impact on streamflow in small watersheds. Sci. Total Environ. 440, 33–41.
Tramblay, Y., Koutroulis, A., Samaniego, L., et al., 2020. Challenges for drought assessment in the Mediterranean region under future climate scenarios. Earth-Sci. Rev., 103348
Tuel, A., Eltahir, E.A.B., 2020. Why is the Mediterranean a climate change hot spot? J. Clim. 33 (14), 5829–5843.
UN, 2021. World Water Development Report 2021 "Valuing Water". UNESCO, Paris.
van Meijgaard, E., van Ulft, B., van de Berg, W. J., Bosveld, F. C., van den Hurk, B., Lenderink, G., and Siebesma, A. P.: The KNMI regional atmospheric climate model RACMO version 2.1 (KNMI TR-302), Tech. Rep., Technical Report TR-302, 2008.
Van Vuuren, D.P., Edmonds, J., Kainuma, M., et al., 2011. The representative concentration pathways: an overview. Clim. Change 109, 5–31.
Voldoire, A., Sanchez-Gomez, E., Salas y Mélia, D., et al., 2013. CNRM-CM5.1 global climate model: description and basic evaluation. Clim Dyn 40, 2091–2121. https://doi.org/10.1007/s00382-011-1259-y.
Wilby, R.L., Dessai, S., 2010. Robust adaptation to climate change. Weather 65 (7), 180–185.
Wilks, D.S., 1995. Statistical Methods in Atmospheric Science, volume 59 of International Geophysics Series. Academic Press, San Diego, London.
Willkofer, F., Schmid, F.J., Komischke, H., et al., 2018. The impact of bias correcting regional climate model results on hydrological indicators for Bavarian catchments. J. Hydrol. Reg. Stud. 19, 25–41.
Xie, S.P., Deser, C., Vecchi, G.A., et al., 2015. Towards predictive understanding of regional climate change. Nat. Clim. Change 5 (10), 921–930.
Yu, G., Wright, D.B., Li, Z., 2020. The upper tail of precipitation in convection-permitting regional climate models and their utility in non-stationary rainfall and flood frequency analysis. Earth's Future 8 (10) e2020EF001613.
Zittis, G., Hadjinicolaou, P., Klangidou, M., et al., 2019. A multimodel, multi-scenario, and multi-domain analysis of regional climate projections for the Mediterranean. Reg. Environ. Change 19, 2621–2635.